# Permafrost Thaw and Ground Settlement Considering Long-Term Climate Impact in Northern Alaska

**Joey Yang** ( zyang2@alaska.edu )
University of Alaska Anchorage https://orcid.org/0000-0001-6387-941X
**Kannon C. Lee**
PND Engineers, Inc
**Haibo Liu**
Columbia University

**Research Article**

**Keywords:** Permafrost thaw, ground settlement, long-term climate impact, thermal modeling, Northern Alaska

**Posted Date:** February 18th, 2021

**DOI:** https://doi.org/10.21203/rs.3.rs-207708/v1



**Version of Record:** A version of this preprint was published at Journal of Infrastructure Preservation and Resilience on April 13th, 2021. See the published version at https://doi.org/10.1186/s43065-021-00025-2.

# Permafrost thaw and ground settlement considering long-term climate impact in Northern Alaska

Zhaohui Joey Yang[1*], Kannon C. Lee[2], and Haibo Liu[3]

[1] Civil Engineering Department, the University of Alaska Anchorage, 3211 Providence Dr., Anchorage, AK, 99508. Email: zyang2@alaska.edu

[2] PND Engineers, Inc., 1506 W. 36th Ave., Anchorage, AK 99503. Email: KLee@pndengineers.com

[3] Columbia University, New York, NY 10964; e-mail: hbl6804@gmail.com

*Corresponding author

**Abstract**

Alaska's North Slope is predicted to experience twice the warming expected globally. When summers are longer and winters are shortened, ground surface conditions in the Arctic are expected to change considerably. This is significant for Arctic Alaska, a region that supports surface infrastructure such as energy extraction and transport assets (pipelines), buildings, roadways, and bridges. Climatic change at the ground surface has been shown to infiltrate soil layers beneath through the harmonic fluctuation of the active layer. Past studies found that warmer air temperature resulted in increasingly deeper thaw, leading to a deeper active layer. This study attempts to assess climate change based on the climate model data from the fifth phase of the Coupled Model Intercomparison Project and its impact on a study site on the North Slope. The predicted air temperature data are analyzed to evaluate how the freezing and thawing indices will change due to climate warming. A thermal model was developed that incorporated a ground surface condition defined by either undisturbed intact tundra or a gravel fill surface and applied climate model predicted air temperatures. Results indicate similar fluctuation in active layer thickness and values that fall within the range of minimum and

maximum readings. It is found that the active layer thickens when the ground surface is either gravel fill or undisturbed tundra, but its thickness varies based on climate model predictions. These variations in active layer thickness are then analyzed by considering the near-surface frozen soil ice content. Analysis of results indicates that strain is most significant in the near-surface layers during thaw, indicating that settlement would be concurrent with annual thaw penetration. From this study, the climate model predicted air temperatures for a warming Arctic suggest that the thaw of near-surface frozen ground is largely dependent on ground surface conditions and the thermal properties of soil. Moreover, ice content is a major factor in the settlement predictions on Alaska's North Slope. This study's results can help enhance the resilience of the existing and future new infrastructure in a changing Arctic environment.
**Keywords:** Permafrost thaw; ground settlement; long-term climate impact; thermal modeling; Northern Alaska

## Introduction

Permafrost is rock, sediment, or other earth material remaining below 0°C for two or more years. At present, it occupies 24% of the land area of the northern hemisphere. Permafrost can be very thick from 500 to 1400 m to very thin at several meters or less [1], and its temperature can vary from lower than -10°C in the Arctic to within 1 to 2°C of the melting point in the sub-Arctic. Permafrost occupies two main zones: continuous and discontinuous (includes the sporadic zone). In a continuous zone, permafrost occupies an entire area except beneath lakes and rivers, whereas in a discontinuous zone, it occupies between 10 and 90% of the area [2,3]. The top layer above the permafrost, which thaws in the summer and freezes in winter, is termed as the active layer and, on average less than 1 m thick in the Arctic region [1].

The consensus among researchers is that global climate warming will be greatest at high-latitude regions [4-8]. Warming air temperatures, as evident from airport weather station direct temperature measurements gathered over the past 100 years in Alaska's Arctic, show a dramatic increase beginning in the 1980s. The 2018 Arctic Report Card published by National Oceanic and Atmospheric Administration indicated a rise in air temperature throughout the Arctic, where warming is twice as fast as the global average due to Arctic amplification [9]. And the annual average air temperature in the Arctic from October 2017 through September 2018 was the second-highest on record.

As air temperatures in the Arctic increase over time, ground temperatures rise, resulting in thaw of the permafrost nearest the surface. Changes to the ground surface significantly affect the permafrost thaw. The vegetative cover at the ground surface acts as an insulating blanket and the first line of defense against permafrost thaw. Linell [10] evaluated the relationship

between vegetative cover and permafrost degradation in a study based in Fairbanks, AK, that lasted 26 years. The study focused on three ground cover conditions: undisturbed natural area, a section cleared of trees and brush, and a section stripped of all vegetative cover. This study found that only the original densely tree-covered section remained free from permafrost degradation and the other two sections had an increased permafrost degradation rate, with the section stripped of all vegetative cover displaying a faster rate. Notably, the thaw degradation process is complex that occurs in various stages and depends on both ground surface conditions and the thermal properties of the soil. Within a column of permafrost, the process of thaw degradation acts on the thermal regime of the soil to cause varying effects. The transient layer, located between the active layer and the permafrost table, can degrade during years of unusually large active layer thickening. Thawing continues as the thickening of the active layer adjusts to the new thermal regime. An increase in the active layer thickness (ALT) can lead to the formation of taliks, which are unfrozen soils trapped within permafrost due to the seasonal freezing at the ground surface. The presence of taliks may cause internal degradation of permafrost where water forms caves and ground water piping networks [11].

Past research [12-20] has measured and modeled temperature change in permafrost due to variation in air temperature. There is a consensus that surface permafrost has warmed over the past century and that an increase in air temperature will result in further degradation. If the air temperature continues to warm, however, the active layer will thicken, causing warmer ground temperatures to penetrate to greater depths. The result is widespread thaw settlement and thermokarst development leading to severe maintenance and repair for the built infrastructure [21].

Development in permafrost regions has occurred at a rapid rate [15,22,23]. For example, the extensive energy infrastructure on Alaska's North Slope, including gravel roads, gravel pads, pipeline networks, is built on continuous permafrost and relies on the sound bearing capacity of the permafrost, which is typically ice-rich and thaw-unstable. Meanwhile, global warming will create unprecedented economic opportunities as an ice-free Northwest passage offers new trade routes through the Arctic Ocean, likely by midcentury. The US Federal Government envisions the Arctic as a new frontier that will thrive due to global warming. Extensive new public infrastructure will need to be built to support the envisioned opportunities. How to enhance the resilience of the existing and future new infrastructure in a changing Arctic environment is crucial to the Arctic regions' social and economic development. It is therefore imperative to assess what effects it will have on permafrost and how these effects directly impact infrastructure built on permafrost-laden soils.

This study focuses on a study site underlain by continuous permafrost. It aims to evaluate the changing thermal regime in the soil layers near the ground surface and predict cumulative settlement and determine the change in freezing and thawing indices due to worst-case air temperature predictions. A thermal model is developed to simulate the effects of air temperature predictions on the near-surface ground thermal regime and to determine the worst-case settlement results based on air temperature predictions.

## Description of the Study Site

The study site (N70°16.25', W 150°06.07') is on the Central Beaufort Coastal Plain of the Alaska North Slope, as shown in Fig. 1, along with all associated landmarks that are referenced in this study. Alluvial marine deposits, floodplain deposits, and eolian sand and loess underlay the flat terrain [15,24,25]. This region supports energy development by multiple oil and gas companies. Gravel access roads, gravel pads, and pipeline networks dominate the landscape. These infrastructures are constructed on continuous permafrost extending several hundred meters deep [26].


Fig. 1 Location of study site on Alaska's North Slope.

The Mean Annual Air Temperature (MAAT) provides an indication of climate change. Locally, the air temperature was measured at the Ugnu Kuparuk Airport, the nearest airport equipped with a National Oceanic and Atmospheric Administration [27] linked weather station. The two additional airport weather stations include Deadhorse to the east and closer to the Beaufort

Sea coast and  Nuiqsut to the west and situated on a floodplain. The study site is located between these other places and approximately the same distance from the sea coast as Deadhorse. Fig. 2 illustrates the historical MAAT data available at Kuparuk, Nuiqsut, and Deadhorse from 1983 to the present, indicating a consistent warming trend at the study site and throughout the region. The MAAT increased from -12 to -8.7°C from 1983 to 2018, corresponding to an annual rate of 0.094°C/yr.

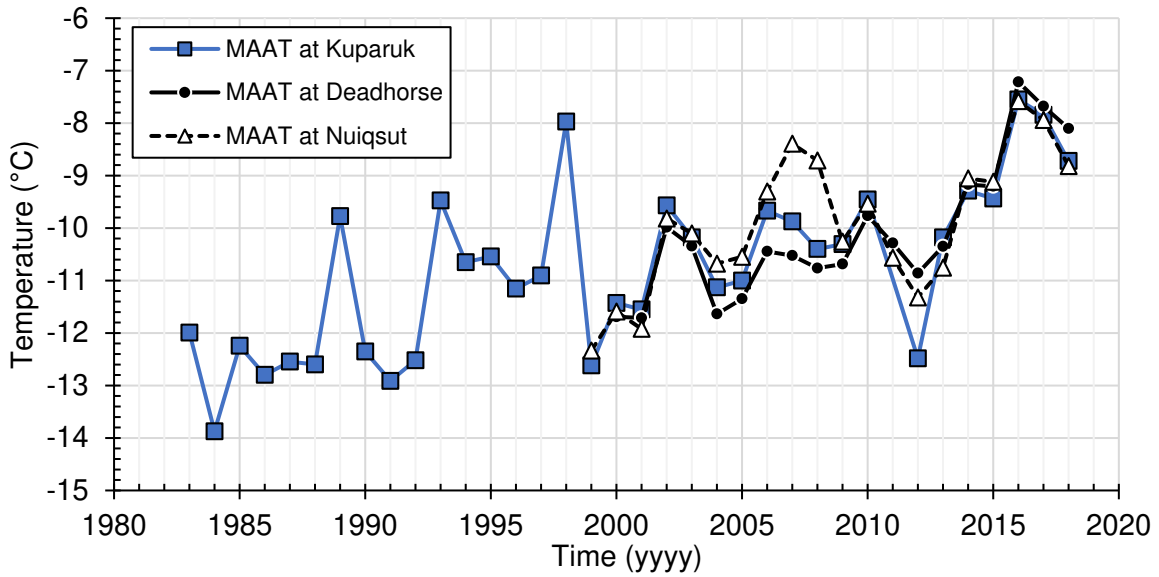


Fig. 2 Mean annual air temperature comparison between locations indicating similar increasing temperature trends.

## Predicted Climate Trend

### MAAT Prediction

The climate models used are a part of the fifth phase of the Coupled Model Intercomparison Project (CMIP5) [28]. The climate models produced a state-of-the-art multimodel dataset designed to advance knowledge of climate variability and climate change. Among the four

greenhouse gas concentration trajectories, Representative Concentration Pathway (RCP) 8.5 is the least optimistic scenario and reflects current global practice, high fossil fuel use, low renewables, and fragmented global cooperation. According to the current consensus regarding greenhouse gas emission levels, the RCP 8.5 is considered the most probable scenario [29]. Thus, this study used RCP 8.5 daily surface air temperature (two m above ground) from all available models

In all, 30 CMIP5 climate models were provided to cover the region near the study site using the RCP 8.5 scenario. The reported surface air temperature was for 2 m above the ground surface. Each model began on 1/1/2006 and ended on 12/31/2099 for a total of 94 years. Fig. 3 depicts the MAAT data of 30 models and their average from 1983 to 2100. MAAT was projected to increase from -8.9 in 2006 to 0.1°C in 2100, correspond to an annual rate of 0.096°C/yr. Each climate model was represented to show the variation in prediction for each year. The historical trend seen on the left portion of Fig. 3 aligns with the average MAAT of the 30 climate models, although the historical trend line does not match up with the average at first. The predicted MAAT result demonstrates an eventual match if the historical trend line is extended into the future, even with the climate models reflecting the worst-case scenario for climate change. Notably, among the 30 models, 28 follow the 365-day calendar and two use the 360-day calendar. The latter present challenges for model input and, hence, were not used in the subsequent ground thermal analyses. The average of the 28 models predicts a similar trend in air temperature as the average of the 30 climate models, as shown in Fig. 3. The 28-climate model average was slightly warmer in prediction, indicating that the two climate models removed predict cooler air temperatures. Beyond focusing on the averages of the climate

models, all predicted MAAT experience fluctuations in warming and cooling. This is important in the analysis of predicted thaw penetration. A decrease in MAAT indicates a recent cooling trend that affects the air freezing index. The freezing index "controls" the maximum thaw penetration allowing for the natural seasonal fluctuation of the active layer.

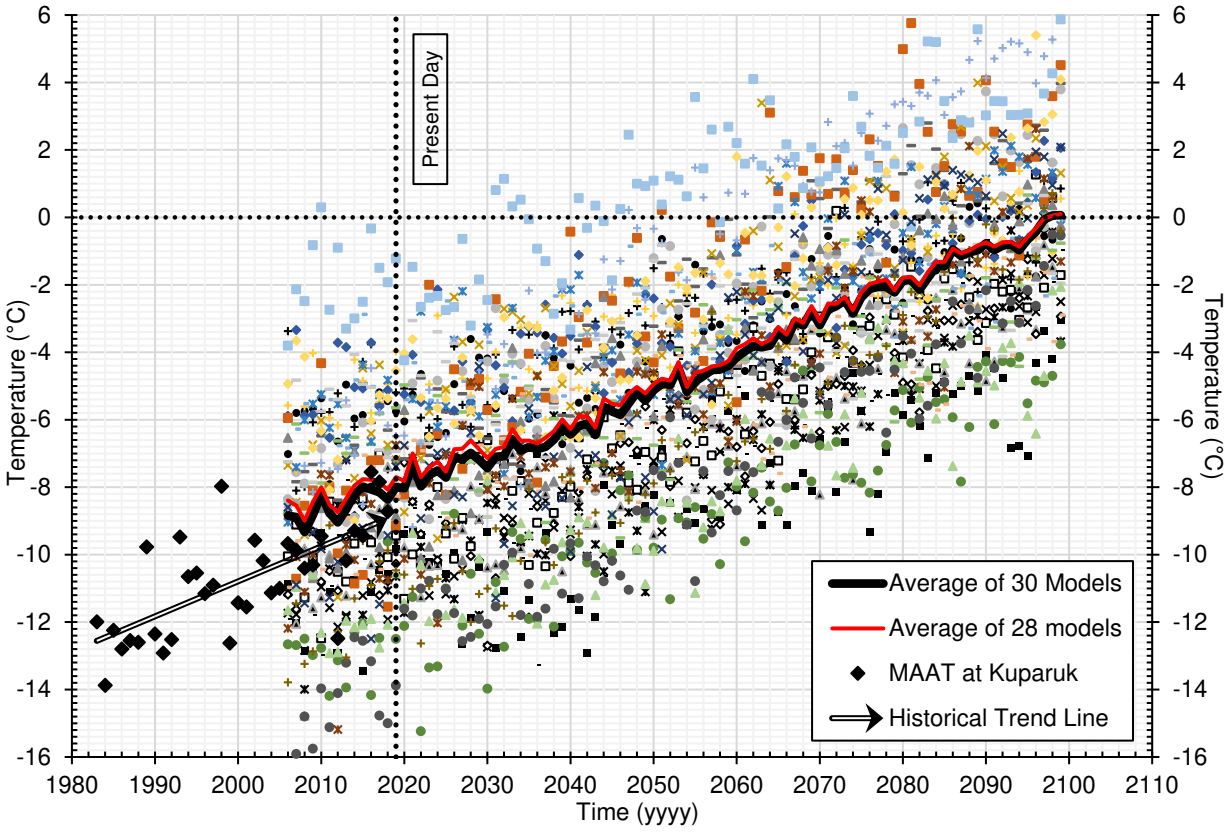


Fig. 3 Historical and predicted mean annual air temperature at the study site. The various colored dots represent 1 of the 30 climate models in this study. The average of all models was used in the thermal modeling.

The MAAT from Fig. 3 was analyzed to determine the upper and lower bounds of air temperature prediction. Fig. 4 provides a closer look at the climate models at the upper and lower bounds of prediction. The four climate models were chosen based on their respective

intensities. Climate model IPSL-CM5A-MR produced the most extreme warming air temperatures at the site; however, its predicted temperature from 2006-2018 is far warmer than the actual temperature readings. On the other hand, BNU-ESM's prediction falls within the historical data scatter and has one of the greatest annual warming rates (i.e., 0.111°C /yr). It reflects the worst-case scenario. A similar visual assessment was made for the lower bound prediction, which was the more conservative outlook. Climate model CMCC-CESM was chosen since its prediction is within the historical scatter with the slowest warming rates, i.e., 0.084°C /yr. The CSIRO-Mk3-6-0 model represents the lowest overall lowest air temperature prediction at the study site, i.e., from -12.7 in 2006 to -3.8°C in 2100; however, the initial air temperature predictions fell well out of the actual historical readings. To summarize, the BNU-ESM climate model and the CMCC-CESM climate model were chosen as the upper and lower bound predictions of air temperatures for the study area, respectively.

Based on Fig. 3 and Fig. 4, the MAAT was predicted to increase by 9°C under the RCP 8.5 scenario. This increase has significant implications for the state of permafrost. The overall prediction was for warmer winter air temperatures, resulting in longer summers and shorter winters. Although all 30 climate models were analyzed for this climate analysis, further comparisons with air temperature during the thaw penetration analysis utilized the 28-climate model average, or the respective upper or lower bound mean daily temperature (MDT).

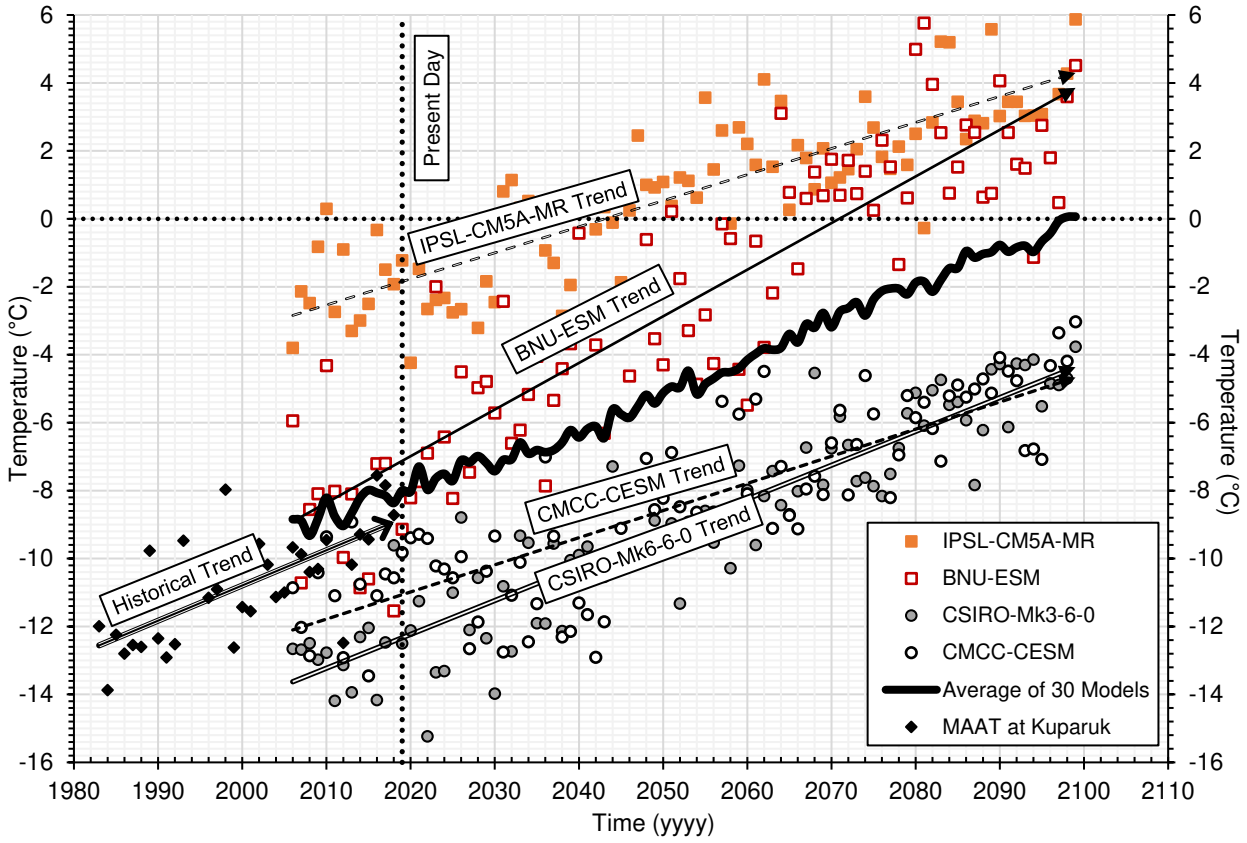


Fig. 4 Predicted mean annual air temperature of the upper and lower bounds of the 30 climate models showing trends of four models with historical and predicted averages.

**Freezing and Thawing Indices**

Air temperature indices, including freezing index (FI) and thawing index (TI), are essential parameters in analyzing the land-climate exchange and for foundation design in permafrost. They are based on air temperatures measured at 1.5 to 2 m above the ground surface. Specifically, the FI (TI) is the number of degree-days below (above) 0°C between the highest and lowest points on the cumulative degree-days time curve for one freezing (thawing) season. The FI determines the thickness of freeze-back of the active layer each year, while the thawing index controls the depth of thaw during the summer months [1]. For this study, these indices were

calculated for each calendar year based on the 30 model predictions from 1983 to 2100. For each year, the average air temperature per month was multiplied by the number of days. The summation of negative degree-days provided the FI, while the summation of positive degree-days provided the TI.

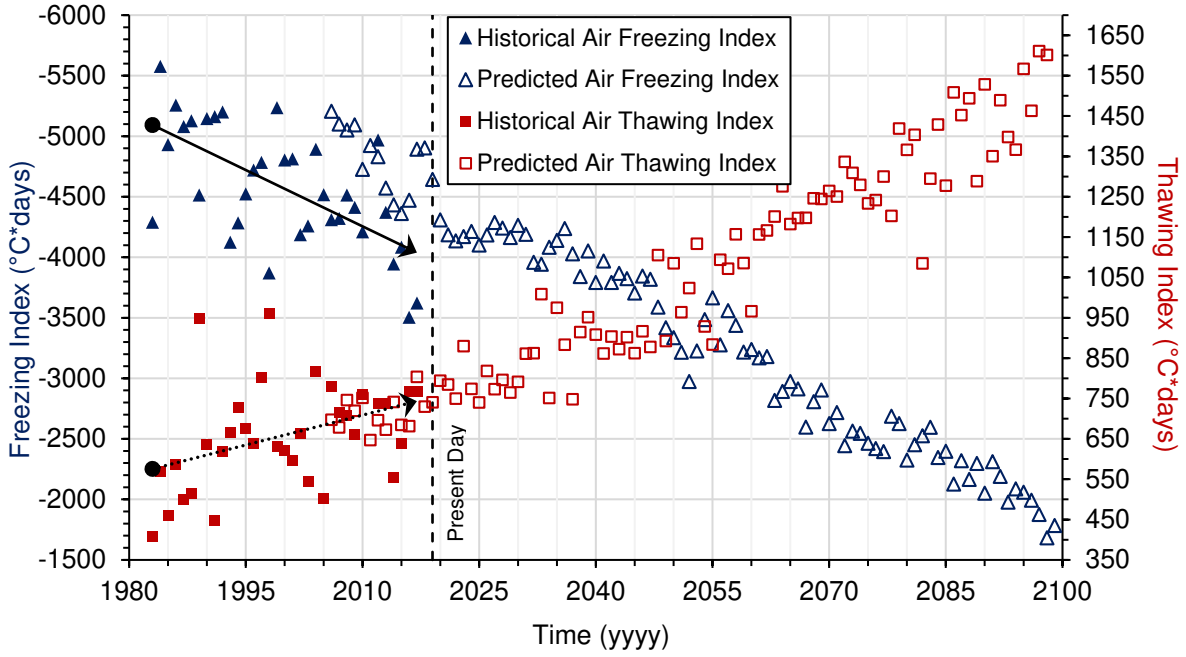


Fig. 5 Historical and predicted air freezing and thawing indices.

On trend, the TI increases, which correlates to a decreasing FI [1]. The trends of both the predicted air indices align well with the historical. The number of days below freezing is thus decreasing, leading to warmer and shorter winters. The decrease in the FI will have a large effect on foundation stability in the Arctic. From 1984 to 2017, the FI range has decreased from 5,577 to 3,622°C-days, or by 54%. Predicted air temperature data indicated that the FI will decrease by 209% (5207 to 1683°C-days) and the TI will increase by 145% (697 to 1706°C-days) from 2006 to 2100. These changes are substantial for the Arctic. Historically, the FI has been larger, which allowed a natural control of ALT because the ground remained frozen for longer

periods of time during the year. When the FI drops, additional engineering measures are needed to prevent thaw settlement from occurring. Thermosyphons are an engineering measure that stabilizes frozen ground by pulling heat from the ground and dispersing it into the air during winter, when the air temperature is cooler than the ground temperature. Predicted air temperature suggests that this balance will tip in favor of warmer air, resulting in much decreased cooling capacity of thermosyphons. Currently, these devices work well with freezing degree days of 3000 to 4000°C-days. They can be retrofitted to increase capacity to account for a decreasing air FI, but that can only be sustained for so long [30].

### Thermal Modeling

Finite element thermal modeling was conducted using the commercially-available TEMP/W program [31]. The heat transfer governing equation is as follows.

$$\frac{\partial}{\partial x} * \left(k_x A \frac{\partial T}{\partial x}\right) + \frac{\partial}{\partial y} * \left(k_y A \frac{\partial T}{\partial y}\right) + QA = A * \left(C + L * w_V \frac{\partial w_u}{\partial T}\right) * \frac{\partial T}{\partial t} \quad (1)$$

where $T$ is temperature, $k_x$ and $k_y$ are thermal conductivity in the x- and y-directions, respectively, $A$ is the cross-sectional area, $Q$ is an applied boundary flux, $C$ is the volumetric heat capacity, $L$ is the latent heat of water, $w_v$ is the volumetric water content, $w_u$ is the unfrozen water content, and $t$ is time [32]. The model input parameters include thermal conductivity, unfrozen water content, and volumetric heat capacity. In this section, the soil profile and models, boundary conditions at the surface and bottom of the models, and soil thermal properties are described. Notably, the TEMP/W analysis only focused on the thermal regime of the soils and did not account for the resulting thaw settlement experienced from predicted warming air temperature. The models also did not account for snow depth during winter, but instead used a frozen $n$-factor that included snow cover effects.

**Soil Profile and model setup**

The permafrost extended up to 200 m below ground surface (bgs) at the study site. As the thaw penetration is not expected to exceed 15 m in the next century, this study only considered the top 45-m soil column consisting of nine distinct soil layers as depicted in Fig. 6. The soil profile was determined based on testing of samples from Drill Site 2M donated to the University of Alaska Anchorage by ConocoPhillips Alaska. Besides, this study also referenced a nearby drill site [33-34]. The surface of the study site was either undisturbed with an intact organic layer or disturbed with the organic layer replaced with gravel fill. These two models are illustrated side-by-side in Fig. 6, and the index properties of various soil layers are listed in Table 1.

Table 1 Soil index properties important to thermal properties

| Soil Layer | Soil Type | Initial e | $G_s$ | n | Grav. Water Content % | Initial $S_r$ % |
|---|---|---|---|---|---|---|
| 1 | ML | 0.79 | 2.70 | 0.44 | 33.2 | 100.0 |
| 2 | SM | 0.65 | 2.67 | 0.39 | 16.4 | 67.6 |
| 3 | SM | 0.88 | 2.67 | 0.47 | 20.0 | 60.5 |
| 4 | SM | 1.01 | 2.67 | 0.50 | 23.5 | 62.3 |
| 5 | SM | 0.88 | 2.67 | 0.47 | 25.2 | 76.4 |
| 6 | CL | 0.87 | 2.78 | 0.46 | 23.1 | 73.9 |
| 7 | CL | 0.80 | 2.78 | 0.44 | 23.3 | 81.2 |
| 8 | SC | 0.82 | 2.67 | 0.45 | 21.0 | 68.3 |
| 9 | CH | 0.83 | 2.79 | 0.45 | 19.5 | 65.9 |

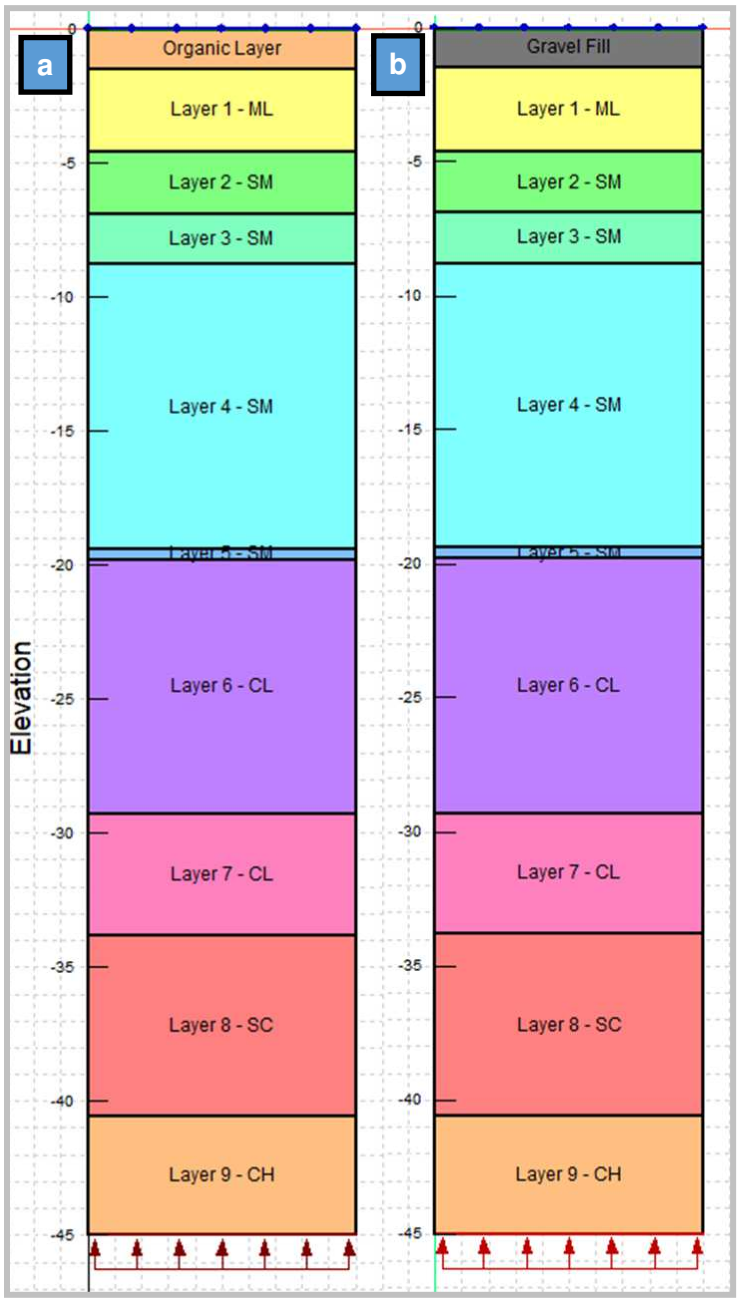


Fig. 6 Comparison of two TEMP/W models: a) with an organic layer at the surface, b) with a gravel layer at the surface.

**Thermal properties**

The thermal conductivity model derived by Johansen [35] was chosen to determine values of thermal conductivity for both frozen ($k_f$) and unfrozen soils ($k_u$). The calculation of $k_f$ utilized the unfrozen water content obtained using the capacitance method [36]. For the ground surface layer (gravel fill or organic material), published values of thermal conductivity were used. The volumetric heat capacity for frozen, $C_f$, and unfrozen, $C_t$, soil was determined based on the weighted average method [1]. Thermal diffusivity, $\alpha$, is based on the ratio of thermal conductivity to heat capacity. More details of thermal property evaluation can be found in Kannon [37]. Table 2 summarizes the thermal properties.

Table 2 Thermal properties of each layer used in this study.

| Soil Layer | Depth bgs m | Soil Type | Thermal Conductivity | | Volumetric Heat Capacity | | Thermal Diffusivity | |
|---|---|---|---|---|---|---|---|---|
| | | | $k_f$ (*-10°C) W/m -°C | $k_u$ W/m -°C | $c_{vf}$ kJ/m$^3$ -°C | $c_{vu}$ kJ/m$^3$ -°C | $\alpha_f$ m$^2$/s x $10^{-7}$ | $\alpha_u$ m$^2$/s x $10^{-7}$ |
| G | 1.5 | GW-GM | 2.15 | 1.49 | 1280.00 | 1804.80 | 13.5 | 6.6 |
| T | 1.5 | OL | 1.20 | 0.60 | 1260.00 | 2700.00 | 4.5 | 1.0 |
| 1 | 4.6 | ML | 2.09 | 1.65 | 3000.10 | 4647.10 | 5.2 | 2.7 |
| 2 | 6.9 | SM | 2.37 | 1.85 | 2315.97 | 3257.79 | 8.8 | 4.9 |
| 3 | 8.8 | SM | 2.01 | 1.52 | 2080.83 | 2958.42 | 8.0 | 4.3 |
| 4 | 19.4 | SM | 1.99 | 1.43 | 2031.53 | 2936.68 | 7.9 | 3.9 |
| 5 | 19.8 | SM | 2.46 | 1.63 | 2243.67 | 3306.87 | 8.7 | 3.9 |
| 6 | 29.3 | CL | 1.34 | 1.13 | 2158.20 | 3265.67 | 5.1 | 2.8 |
| 7 | 33.8 | CL | 1.44 | 1.22 | 2298.60 | 3504.47 | 5.1 | 2.8 |
| 8 | 40.6 | SC | 2.27 | 1.64 | 2224.81 | 3207.73 | 8.4 | 4.2 |
| 9 | 45.0 | CH | 1.27 | 1.10 | 2071.58 | 3063.52 | 5.1 | 3.0 |

**The Land-Climate Exchange**

The type of ground cover has a significant impact on thaw penetration and acts as the first line of defense against climatic changes [11]. This study does not address ground surface characteristics such as vegetation height, snow depth in winter, or water content variation due to precipitation, all of which heavily affect the flow of heat through the ground surface. Instead, the empirical *n*-factor is applied to estimate the soil surface temperature. The *n*-factor is defined as the ratio of the ground FI (or TI) to the air FI (or TI) [1]. The ground cover at the study site was similar to that at the Circumpolar Active Layer Monitoring (CALM) site at Deadhorse, Alaska (N 70°09.677', W 148°27.918'). Note that the CALM program began in 1991 to observe the response of the active layer and near-surface permafrost to climatic changes over the long-term [38]. Based on the ground and air temperature data at Deadhorse from 2001 to 2018, the average thawing and freezing *n*-factors were determined to be 1.0 and 0.5, respectively. These factors will be applied to the thermal modeling to establish the land-climate interaction at natural ground surface conditions. The thawing *n*-factor, 1.0, compares to the findings of Klene et al. [24,25] Cable et al. [39]. The freezing *n*-factor was not evaluated by these studies but deemed appropriate considering the weather conditions and ground cover present on the North Slope.

**Boundary conditions and model scenarios**

The mesh applied to the model consisted of 2938 quadrilateral elements of the same size. In Fig. 6, the circular nodes at the top of the model represent the surface boundary condition, which was the air temperature modified by n-factors. The two models had different freezing and thawing *n*-factors as shown in **Error! Reference source not found.**3. The air temperature

function used was either historical data or predicted mean daily air temperature data as explained previously. The arrows at the bottom represent the heat flux due to the geothermal gradient, i.e., 0.0257 W/m$^2$*),* based on field measurement [34]. Initial ground temperature conditions were based on a USGS study that took place in 1987 in borehole WSak-14 located 5.95 km northeast of the study site.

The "Initial" model using historical air temperature was a separate TEMP/W solution, using the organic layer and tundra vegetative cover ground conditions at the surface. The subsequent models used this initial analysis beginning at step 6669, which was December 31, 2005, the day before the CMIP5 predicted data began. There was a total of six model scenarios that used the "Initial" TEMP/W model as summarized in Table 3. Since the iterations all drew from the initial model, the mesh properties had to be consistent throughout all models. TEMP/W will not allow a model to draw initial temperature conditions from an analysis that has different mesh properties. For example, because the initial analysis was the block structure shown in Fig. 6a, all subsequent models had the same geometry. For this reason, no additions to the soil column models were made that reflected development at the site (i.e., no gravel pad height above the ground surface, no organic layer between the gravel fill and Layer 1).

Table 3 TEMP/W model iterations in this study

| Model | Scenario | Ground Surface Condition | *n*-factor | | Air Temperature Data |
|---|---|---|---|---|---|
| | | | $n_f$ | $n_t$ | |
| | Initial | | | | Historical |
| Undisturbed | 1 | Organic layer and tundra | 0.5 | 1 | Average of 28 CMIP5 Models |
| Tundra | 2 | | | | Upper Bound (BNU-ESM) |

| | | | | | |
|---|---|---|---|---|---|
| | 3 | vegetative cover | | | Lower Bound (CMCC-CESM) |
| Gravel Road | 4 | Gravel fill and maintained surface | 0.95 | 1.25 | Average of 28 CMIP5 Models |
| | 5 | | | | Upper Bound (BNU-ESM) |
| | 6 | | | | Lower Bound (CMCC-CESM) |

All iterations used one-day time steps. The initial model ran for 30 years for a total of 11,010 steps and saved results every step. The model began on August 26, 1987, and ended on December 31, 2018. The start date coincided with the initial temperature conditions established at WSak-14 on August 26, 1987. The predicted iteration models ran for 94 years, for a total of 34,309 steps and saved results every step. Saving results at every step allowed for data extraction on an annual basis.

### Thaw Strain Evaluation Models

Volumetric change of a thawing soil results from the phase change of ice to water and the eventual draining of water out of the soil. Nelson et al. [40] compiled thaw strain values derived from frozen soil index properties. The data was derived from 1024 laboratory tests completed on samples obtained from boreholes drilled along the Trans-Alaska Pipeline System. They conducted a regression analysis of the thaw strain versus frozen soil index properties, including porosity (*n)*, degree of saturation ($S_r$), and gravimetric water content (*w)*, and produced equations for different soil categories to predict representative thaw strain dependent on soil dry density. However, the application of these equations for the soils in this study yielded values that were not comparable to tested values obtained in this study [37]. For this reason, a simple model was developed to determine thaw strain by soil dry density. Fig. 7 and Fig. 8 are

plots of results from this study for silt and clay, and sand and silty sand, respectively, and include results from Nelson et al. [40] and EBA [33]. For each plot, a best-fit function was applied to the data. The correlation coefficient was 0.74 For silt and clay and 0.55 for sand and silty sand.

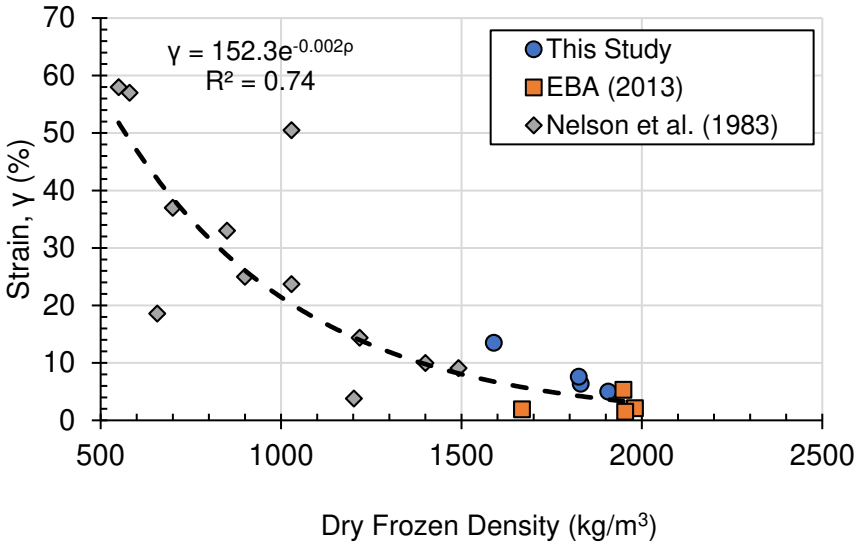


Fig. 7 Percent strain as related to dry frozen density for silt and clay.

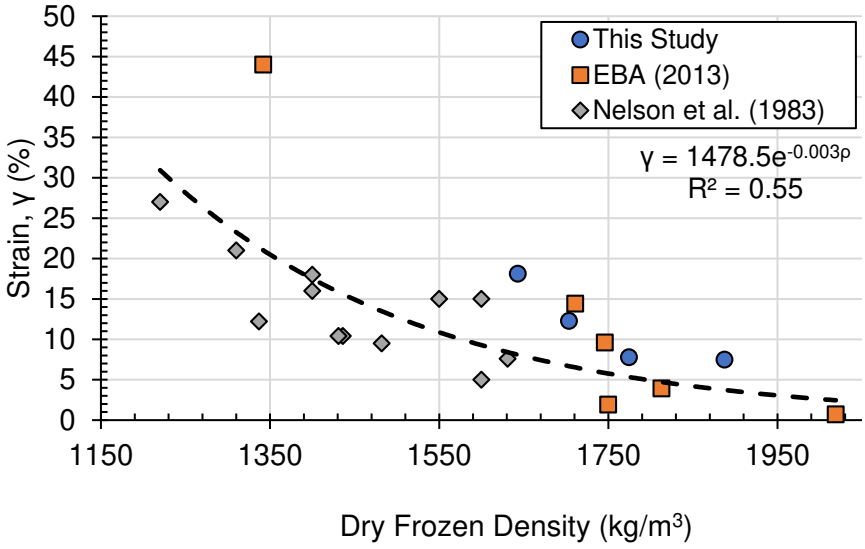


Fig. 8 Percent strain as related to dry frozen density for sand and silty sand.

For this study, the maximum and minimum settlement predictions were determined based on

either ice-rich or ice-poor ground conditions, respectively. In the case of an ice-rich condition, strain values were obtained that correspond to the highest strain within the given range of values; however, in the case of ML, the choice was the average of the three largest strain values due to the difference in density for the highest strains. For the ice-poor condition (Lower Bound), the curve of best fit was used to approximate the strain value. The Lower Bound values of strain differed for the three SM layers where the model indicated thaw penetration. **Error! Reference source not found.** is a summary of the percent strain used in the settlement prediction.

Table 4 Lower and upper bound strain values in this study.

| Soil Layer | Soil Type | Lower Bound | Upper Bound |
|---|---|---|---|
| Surface Condition | GW-GM | 2.0 | 15.0 |
| Surface Condition | OL | 10.0 | 40.0 |
| Layer 1 | ML | 6.0 | 55.3 |
| Layer 2 | SM1 | 4.0 | 44.0 |
| Layer 3 | SM2 | 7.0 | 44.0 |
| Layer 4 | SM3 | 7.6 | 44.0 |

## Thermal Modeling Results

The results presented herein illustrate modeled maximum thaw penetration that occurred during the summer months. The date of maximum thaw penetration did not always correspond to the expected date of maximum thaw, such as the end of August to the beginning of September for the referenced CALM sites. The thermal model is first calibrated by comparing the model-predicted ALT beneath undisturbed tundra using historical air temperature from the Ugnu Kuparuk Airport from 1988-2018 with the observed values. Then the calibrated model was used to investigate the thermal status of the two cases, i.e., disturbed tundra and gravel road, during the observation period of 2006-2100.

**Comparison of Modeled Results to Regional Measurements**

The CALM sites located nearest to the study site are (in order of proximity): Betty Pingo Wet, Deadhorse, and West Dock (refer to Fig. 1). These sites have been continuously monitored since 1995. A comparison was made through an analysis of thermal properties and ground surface conditions. Fig. 9 is a comparison of maximum ALT of the measured and modeled maximum. Betty Pingo Wet is expected to have a shallow ALT due to wet surface conditions, and the deepest ALT was 0.67 m measured in 2017. West Dock, close to the Beaufort Sea, had a maximum ALT of 1.135 m in 2015. Among these three sites, Deadhorse has the most comparable ground surface conditions to the study site and is located at a similar latitude. While the study site has a surficial organic layer thickness of 1.5 m, Deadhorse has a 0.23 m think surficial organic layer. At Deadhorse, the organics were underlain by silt, transitioning to sandy silt at 0.92 m bgs. The maximum ALT reached 0.94 m and fluctuated around the sandy silt interface, suggesting that soil properties may contribute to thaw penetration depths. In

contrast, at the study site, all modeled active layer fluctuations occurred within the homogenous organic layer, which may have contributed to a deeper maximum thaw penetration of 1.18 m in 2017.

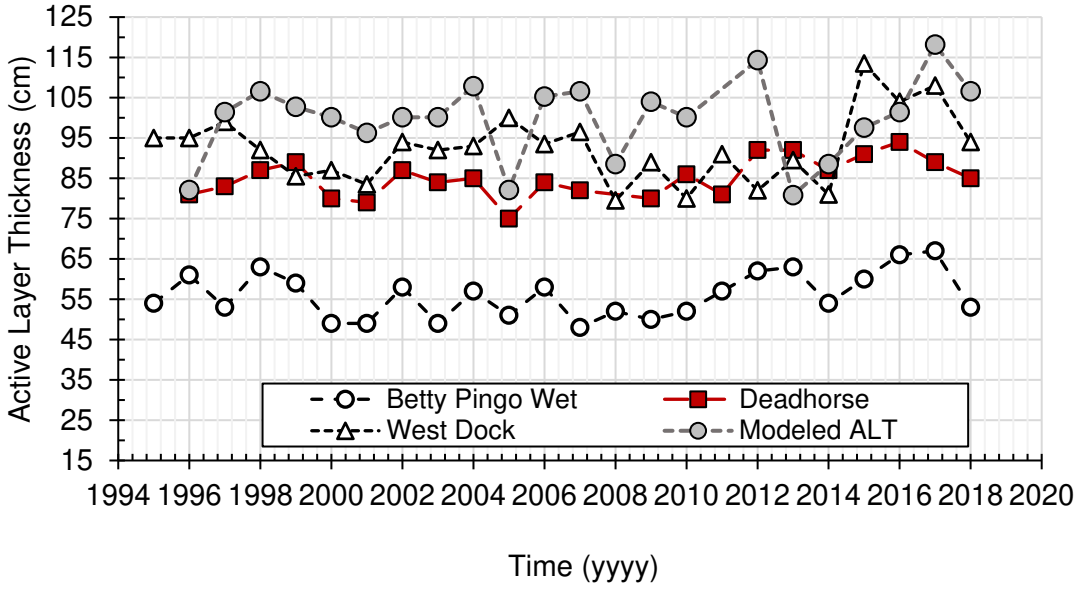


Fig. 9 Comparison of measured and modeled ALT.

**ALT from Predicted Climate Data for Undisturbed Tundra Model**

Fig. 10 is a graph detailing the effects of the three climate model scenarios on the ALT for undisturbed tundra. All predictions began with the initial historical air temperature data indicating that the choices for upper and lower bounds of climate model air temperature predictions were appropriate. The fluctuation of the ALT is natural, indicating a response to annual average temperature. For the modeled results, ALT fluctuation was apparent for all climate scenarios for the first half of the observation period.

For Scenario 1 (Average), the inclusion of warmer summers and shorter winters from all climate models caused the ALT to fluctuate with increasing amplitude over time. By the end of the 21$^{st}$ century, the ALT decreased by 23% from 2080 to 2090 and increased by 93% from 2090 to

2095. This fluctuation indicated that air temperatures may be experiencing substantial minimum and maximum extremes, causing this erratic shift in amplitude. Overall, the ALT increased by 109% (1.00 to 2.09 m). Scenario 1 may be the best estimate of climate predictions for the North Slope since it combines all 28 climate models. The results from Scenario 2 (Upper Bound) demonstrated some fluctuation during the early observation period, but the decline in fluctuation was rapid with the onset of warmer air temperature. Overall, the ALT increased by 496% (1.14 to 6.79 m).

For Scenario 3 (Lower Bound), the ALT did not exceed the organic layer. The ALT was more sensitive to freezing air temperature because this climate scenario was on the lower end of climate model predictions. As a result, the ALT was stable, demonstrating a similar response to air temperature as produced by the historical data. The ALT increased by only 37% (0.99 to 1.36 m). This scenario is the most optimistic for the North Slope, and the modeled results suggest that near-surface permafrost beneath undisturbed ground surfaces will not degrade.

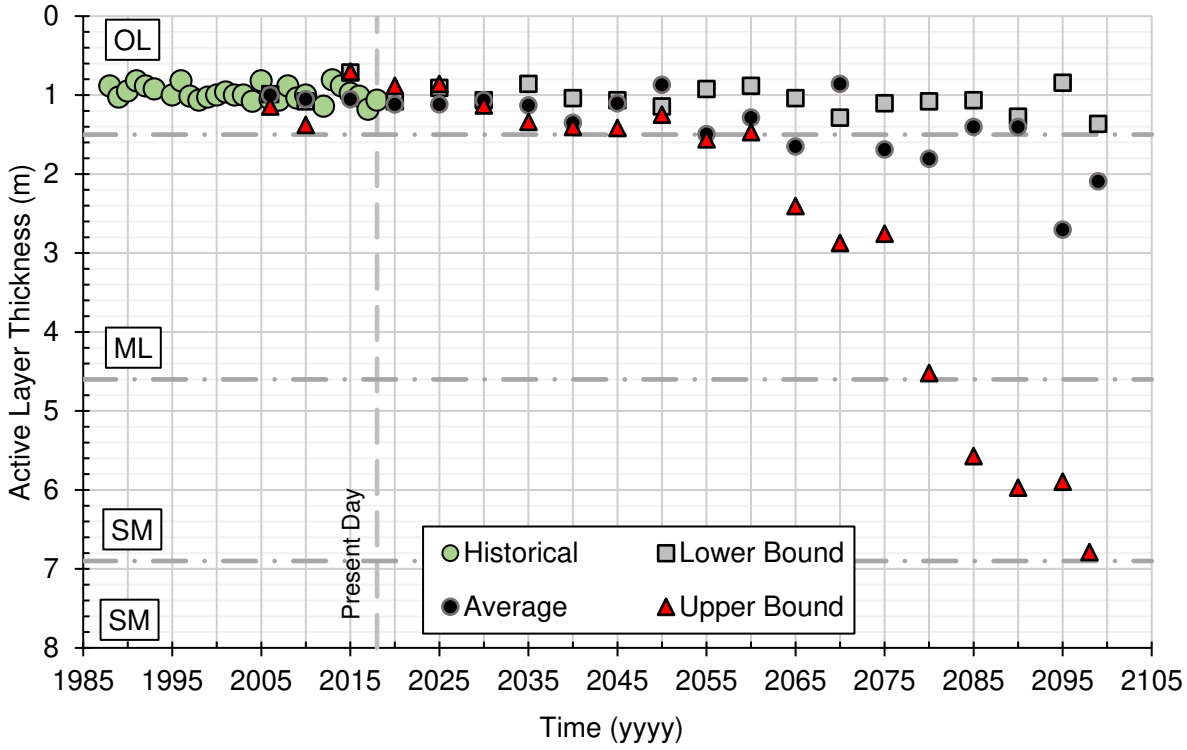


Fig. 10 Modeled ALT from 1988 to 2100 for undisturbed tundra. Scenarios 1, 2, and 3 are represented by Average, Upper Bound, and Lower Bound in the figure, respectively.

**ALT from Predicted Climate Data for Gravel Surface Model**

This model follows the development of the study site beginning with the CMIP5 data in 2006. Gravel pads on the North Slope are placed on the ground surface at 1.5 m thickness and allowed to consolidate for one year [41]. In the thermal model, the organic layer was completely replaced with the 1.5-m thick gravel layer. It is important to note that the thermal modeling block figures represent a one-dimensional single column of material and do not consider any interaction between the edge of the gravel pad and the tundra. The modeling also does not consider effects due to oil drilling activity. Fig. 11 depicts the results of the three climate scenarios on the ALT when a gravel pad is emplaced at the surface; the historical modeled

organic layer ALT is provided in the Fill layer as a reference.

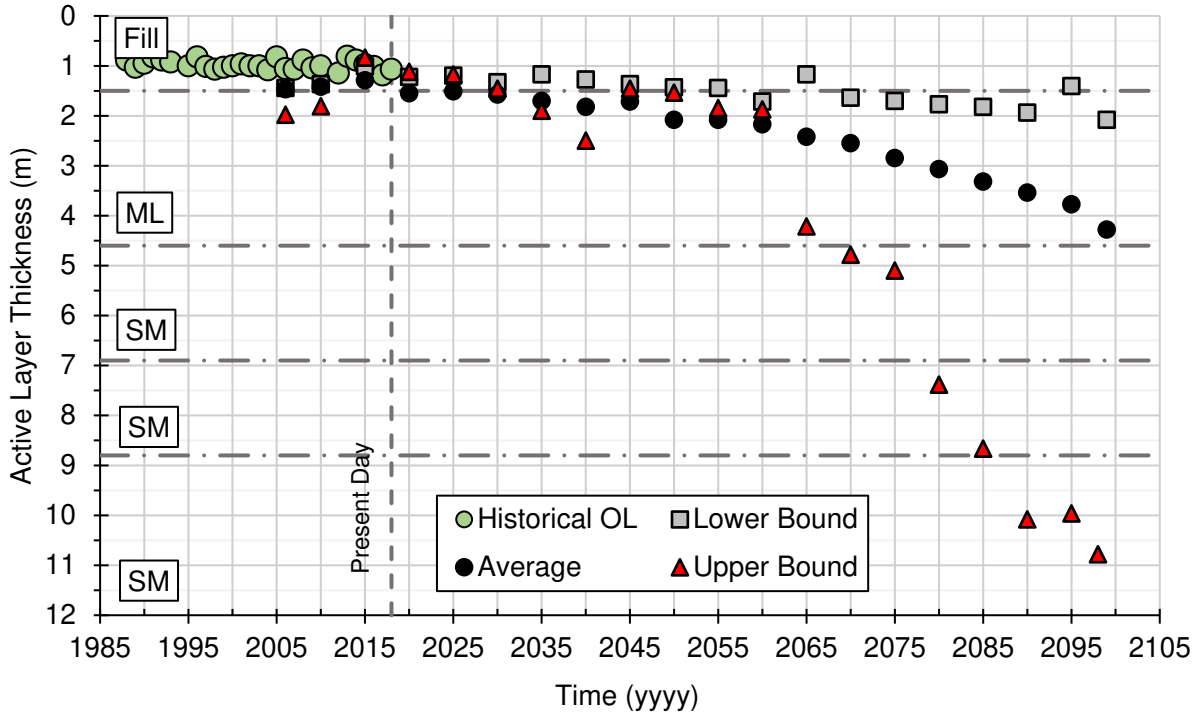


Fig. 11 Modeled ALT when a gravel pad is emplaced at the site, with development occurring in 2006. The modeled historical organic layer ALT is provided for reference. Scenarios 1, 2, and 3 are represented by Average, Upper Bound, and Lower Bound in the figure, respectively.

All models began with a deeper ALT than those modeled using historical air temperature data, indicating that the gravel fill surface thaws quickly during the summer months and may not be thick enough to prevent permafrost degradation at current conditions. For the discussion in ALT change, the average ALT was considered 1.00 m to coincide with modeled historical organic layer ALT. For Scenario 1 (Average), the ALT fluctuated with average annual air temperature, until 2060 when the ALT began to increase substantially. The ALT increased from 1.00 m to 4.30 m by 2100, or by 330%. For Scenario 2 (Upper Bound), the fluctuation amplitude was the

highest, with ALT penetrating into the underlying ML soil. The ALT increased by 980% (1.00 to 10.78 m). For Scenario 3 (Lower Bound), the ALT was fairly stable until 2055 when it began to advance. The ALT increased by 108% (1.00 to 2.08 m).

### Settlement Prediction

Prediction of settlement is just one effect of active layer thickening and serves as the example of what may occur due to a warming Arctic. The modeled ALT from Scenario 2 (Upper Bound) climate predictions suggests substantial thawing may occur by the end of the 21$^{st}$ century. One way that the ground surface can respond to thawing is thaw settlement. Thawing of the near-surface soil layers and melting of excess ice will result in the release of substantial water, which correlates to strain. Settlement prediction, $\delta$, was determined using Equation 17:

$$\delta = \gamma * \Delta\xi \tag{2}$$

where $\gamma$ is strain and $\Delta\xi$ is the thaw penetration increment prediction between evaluation years; five-year increments were used, unless otherwise noted. Each change in thaw depth increment was multiplied by the thaw strain of the respective soil layer. The calculation of settlement per layer continued from 2006 to 2100 and a cumulative settlement was determined. The cumulative settlement did not factor in any ALT recovery; instead, a value of 0 m was assigned to that year. Predicted settlement from the initial historical model was not factored into overall cumulative settlement.

**Predicted Settlement for the undisturbed tundra model**

Fig. 12 illustrates the predicted settlement of the undisturbed ground surface for each of the modeled climate scenarios. The total settlement differed by climate scenario and followed the intensity of predicted warming. The settlement was predicted under all scenarios but was more

pronounced for the average and upper bound climate scenarios (Figs. 12a and 12b, respectively). And settlement only occurred in the OL surface layer under Scenarios 1 and 3.

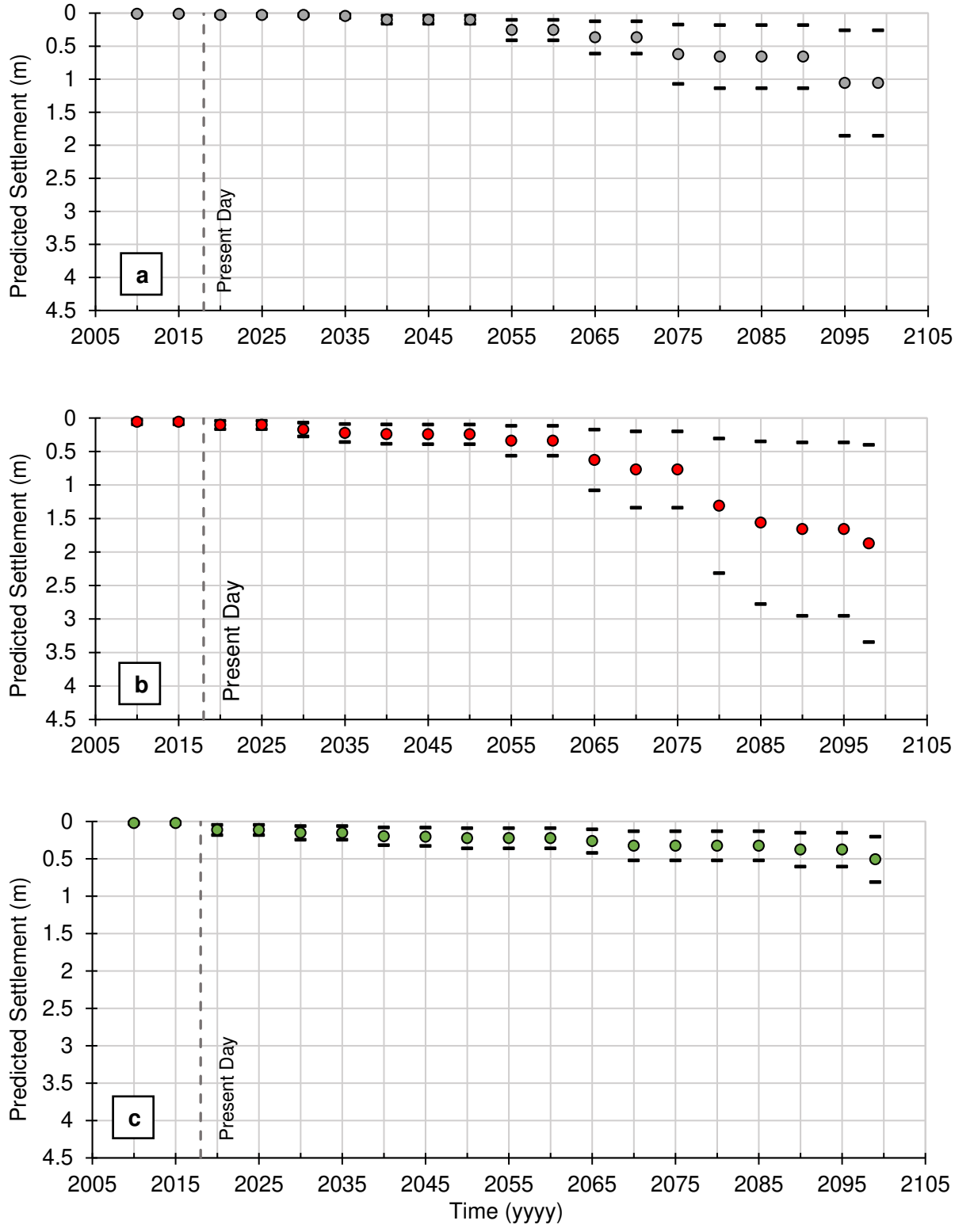

Fig. 12 Predicted settlement at the study site due to active layer thickening under undisturbed ground surface conditions: (a) 28 Climate Model Average; (b) BNU-ESM upper bound climate model; (c) CMCC-CESM lower bound climate model. The dashed vertical line at 2018 indicates the present day for reference.

Organic soil settlement is mainly due to drainage resulting in densification. Thaw penetration to deeper depths allows for the organic layer to drain more readily. Erosion due to water runoff typically is not a problem for organic soil, unless coarser soil layers beneath are exposed [42]. Fig. 12b indicates this shift in settlement stability at 1.5 m bgs when predicted settlement reaches the ML layer. Also, in Fig. 12b, the predicted settlement levels off in 2080, which coincides with the ALT reaching the first SM layer. In all cases, the range of predicted settlement steadily increases over time.

**Predicted settlement for the gravel surface model**

Gravel fill substitution represents the construction of roads and gravel pads at the study site. Construction involving gravel fill must occur during the winter to avoid rapid thaw of ground surface conditions. This suggests that gravel fill at the site was placed during a time when the air temperature was below freezing and water in the gravel material was frozen. Placement most likely involved compaction of frozen gravel in which voids were filled with ice and trapped air. Subsequent warming after placement leads to thaw and rearrangement of voids over time. Precipitation and annual freezing and thawing also affect how voids are rearranged. Settlement prediction in the gravel layer may be due to a decrease in the void ratio, leading to densification and reduction in height. Once soil layers below the gravel fill begin to thaw, predicted

settlement increases and does not recover.

The results suggest that removal of the organic layer creates a change to the thermal regime of the underlying soil layers. Fig. 13a and 13c correspond to Scenarios 1 and 3, respectively. These results show predicted settlement remaining in the gravel fill layer, but do not reflect the iterative process needed to predict actual settlement. If thawing penetrates to 1 m bgs, settlement will occur concurrently with thaw. In Scenario 1, predicted settlement is expected to be greater than Scenario 3 due to the inclusion of greater air temperature increases from all 28 climate models. Fig. 13b corresponds to Scenario 2. The results indicate predicted settlement reaching about 5.1 m under ice-rich conditions. Settlement is directly related to the predicted thaw penetration. Therefore, when the active layer thickens to depths below the gravel fill layer, predicted settlement increases when soil is ice-rich. More ground ice present at the site correlates to higher water content. As a result, overburden pressures will have a greater effect on the thawing soil layer. Fig. 13b for the undisturbed tundra scenario also indicates similar depths of settlement. The main difference is that the undisturbed tundra stabilizes while the gravel fill surface shows a progressive advance in the predicted settlement. This, too, does not account for the iterative, cumulative settlement predicted if thaw penetrates 1 m bgs to the permafrost table. The strain for upper bound predictions is high for Layer 1 – ML at 55.3%, indicating that overburden pressure will have an effect on settlement. The thawing of ice-rich soil may result in high pore water pressure. As long as the thaw rate is slow, pore pressure can dissipate; however, if rapid thawing occurs, high pore pressure may reduce soil shear strength, leading to possible foundation and slope failures.

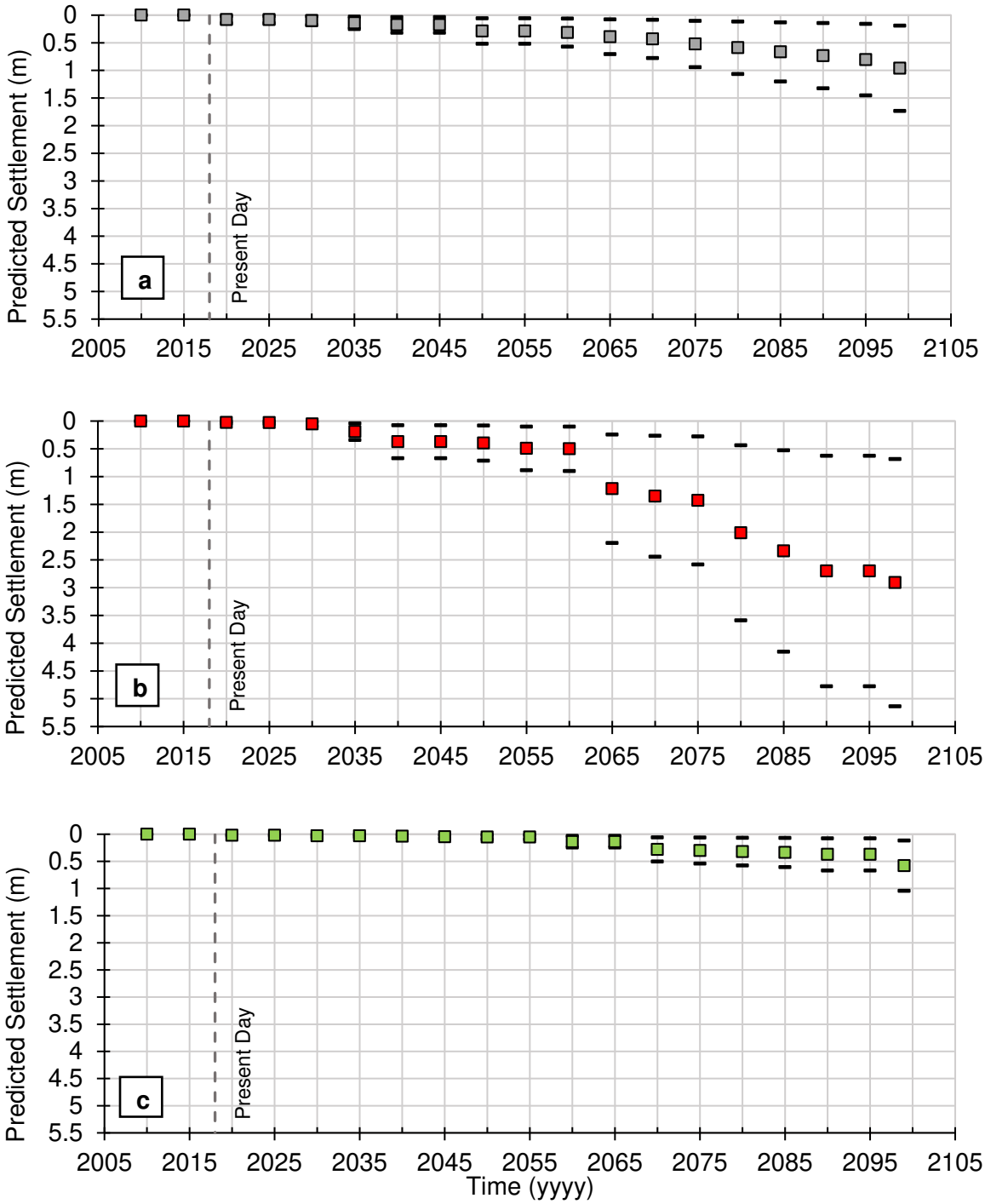


Fig. 13 Predicted settlement at the study site due to active layer thickening under disturbed ground surface conditions where the organic layer was replaced with gravel fill: (a) 28 climate model average; (b) BNU-ESM upper bound climate model; (c) CMCC-CESM lower bound climate model.

**Possible Effects on Infrastructure**

Warming air temperature will affect infrastructure on the ground surface. This is significant for a region that supports surface infrastructure such as energy extraction and transport assets, buildings, roadways, and bridges. For example, pilings initially installed within permafrost may be compromised by permafrost degradation. The effective length of a piling embedded within permafrost will decrease, resulting in more length subjected to frost heave forces and less length affording bearing capacity via adfreeze bonding. The warming of deep and near-ground surface permafrost will increase the creep rate of existing pilings and footings [43]. Esch et al. [43] explained that pilings designed for permafrost temperatures of -4°C will have a 75% loss in load capacity if the temperature at the permafrost table increases to -1°C. This may be an underestimate as the unfrozen water content is also a factor for warm permafrost temperatures approaching the thawing point. In some areas, the ground surface conditions will change completely, with vegetative cover giving way to thermokarst pits that may fill with water, creating thermokarst lakes. For regions closer to the Arctic Coastal Plain Foothills, there may be an increase in downslope soil movement resulting in a greater chance for landslides.

Alaska has more than 7,022 km of paved roads with approximately 60% located in the discontinuous permafrost zone [44]. The majority of paved roads are not constructed in the continuous permafrost zone, but many large airport runways are (i.e., runways at Kotzebue, Deadhorse, Prudhoe Bay, Utquiavik, Kuparuk). The state-wide warming that occurred in the late 1980s led to major thaw settlement of the Deadhorse runway [44]. Predicted warming of air temperatures will only make the situation worst.

Another area of concern is the use of thermosyphons and how they will maintain frozen ground

in a warming climate. The concern is that, with a warming climate, the thermosiphon's cooling capacity is reduced due to a decline in available cold air. The freezing index is used to determine the proper spacing of evaporators for thermosyphon placement and design. For example, a freezing index of 4200°C- days allows spacing of between 0.8 to 1.8 m for a 15.8 $m^2$ condenser thermosyphon. With a decreasing freezing index, however, the required spacing range decreases, rendering the installed thermosyphons incapable of preserving the foundation [30]. Current systems that are inefficient due to warming air temperatures need to be retrofitted to boost the condenser and evaporator area or be replaced altogether.

## Conclusions

In this study, and thermal modeling was conducted to assess the effect of warming air temperature on permafrost and associated ground settlement in Northern Alaska during the next century. The climate model data from the CMIP5 project were analyzed to predict how the freezing and thawing indices will change due to climate warming. Thermal models were developed to evaluate the maximum active layer thickness under two ground cover conditions (i.e., undisturbed tundra and a gravel fill surface) and three separate climate scenarios, which were based on multiple climate model predictions. Using the thermal model results and thaw strain models, surface settlement was calculated for each scenario. The following conclusions can be made based on the research results:

1. Based on the average predicted air temperature from the 30 climate models, the freezing index is predicted to decrease by 209% by the end of the 21st century, with a corresponding increase of 145% in the thawing index. This suggests that near-surface soils will be frozen for shorter periods of time and that measures to sustain frozen ground

conditions year-round will need to be taken.

2. Based on thermal modeling results, the greatest increase in ALT occurred beneath a gravel fill surface under the upper bound climate model prediction, in which the ALT increased by 980% (1.00 to 10.78 m). The smallest increase occurred beneath an undisturbed tundra surface under the lower bound climate model prediction, in which the ALT increased by 37% (0.99 to 1.36 m). These results indicate the importance that ground surface conditions have against the predicted climate scenario intensity.
3. Settlement prediction was more pronounced for the upper bound climate model prediction under an ice-rich soil condition. For the undisturbed and disturbed ground surfaces, the maximum predicted settlements were 3.3 m and 5.1 m, respectively. Substantial predicted warming after 2050 contributed to an increase in the thaw depth and settlement, which may generate excess pore pressures. Results indicated that the ice-rich condition results in the worst-case scenario for settlement.
4. The study results suggest a bleak outlook for surface infrastructure with a warming climate. Increasing ALT will result in thaw of ground ice, leading to settlement at the ground surface. This is significant for a region that supports surface infrastructure such as energy extraction and transport assets, buildings, roadways, and bridges. Current engineering practices will have to evolve to address the predicted thaw of permafrost. For example, with the reduction of the freezing index, the ability to cool frozen ground actively will be reduced, requiring additional engineering measures to stabilize foundations in the Arctic.

During this study, a few areas were identified for further research: 1) Increasing the amount of monitoring sites across Northern Alaska will provide observations of the effect of climate on

permafrost; 2) investigating ground cover conditions by incorporating varying material types to model how the ALT responds over time (i.e., the inclusion of an insulative material like extruded polystyrene or a compressed organic layer); 3) Investigating thaw and post-thaw strain testing to establish an ASTM International standard testing procedure, including designing a device to test thaw and post-thaw strain that restricts upward drainage; and 4) applying an iterative process to cumulative settlement calculation to consider the concurrent settlement occurring at the permafrost table during thaw penetration.

## List of abbreviations

**ALT**: Active Layer Thickness

**MAAT**: Mean Annual Air Temperature

**CMIP5**: Coupled Model Intercomparison Project - Phase 5

**RCP**: Representative Concentration Pathway

**MDT**: Mean Daily Temperature

**FI**: Freezing index

**TI**: Thawing Index

**BGS**: Below ground Surface

**CALM**: Circumpolar Active Layer Monitoring

## References


1. Andersland, O. B., & Ladanyi, B. (2004). Frozen Ground Engineering. (Second, Ed.) ASCE Press/Wiley & Sons.
2. Zhang, T., Heginbottom, J. A., Barry, R. G., & Brown, J. (2000). Further statistics on the distribution of permafrost and ground ice in the Northern Hemisphere. Polar Geography, 24(2), 126-131.
3. Romanovsky, V. E., Smith, S., Yoshikawa, K., & Brown, J. (2002). Permafrost Temperature Records: Indicators of Climate Change. EOS, 83(50), 589-600.
4. Budiko, M. I. (1980). The climate in the past and future. Hydrometeoizdat, 351.
5. Vyalov, S. S., Gerasimov, A. S., & Zolotar, A. J. (1993). Ensuring structural stability and durability in permafrost ground areas at global warming of the Earth's climate. Proceedings of the 6th International Conference on Permafrost (pp. 955-960). Beijing China: South China University of Technology Press.
6. IPCC. (1995). Climate Change 1995: Impacts, Adaptations and Mitigation of Climate Change, Scientific-Technical Analyses. Second Assessment Report of the Intergovernmental Panel on Climate Change (AR2).
7. Anisimov, O. A., Shiklomanov, N. I., & Nelson, F. E. (1997). Effects of global warming on permafrost and active-layer thickness: results from transient general circulation models. Global and Planetary Change, 15(2), 61-77.
8. IPCC. (2014). Climate Change 2014: Impacts, Adaptation, and Vulnerability. Contribution to the Working Group II. Fifth Assessment Report of the Intergovernmental Panel on Climate Change (AR5).

9. Overland, J. E., Hanna, E., Hanssen-Bauer, I., Kim, J., Walsh, J. E., Wang, M., . . . Thomas, R. L. (2018). Arctic Report Card: Tracking recent environmental changes relative to historical records. Retrieved from Arctic Program: https://www.arctic.noaa.gov/report-card.
10. Linell, K. A. (1973). Long-term effects of vegetative cover on permafrost stability in an area of discontinuous permafrost. Proceedings of the 2nd International Conference of Permafrost, North American Contribution (pp. 688-693). Washington D.C.: National Academy of Science.
11. Jorgenson, M. T., Romanovsky, V. E., Harden, J., Shur, Y. L., O'Donnell, J., Schuur, E. A., . . . Marchenko, S. (2010). Resilience and vulnerability of permafrost to climate change. Canadian Journal for Research, 40, 1219-1236.
12. Goodrich, L. E. (1978). Some results of a numerical study of ground thermal regimes. Proceedings of the 3rd International Conference on Permafrost. 1, pp. 29-34. National Research Council of Canada.
13. Lachenbruch, A. H., & Marshall, B. V. (1986). Changing Climate: Geothermal evidence from permafrost in the Alaskan Arctic. Science, 234, 689-696.
14. Anisimov, O. A., & Nelson, F. A. (1996). Permafrost distribution in the Northern Hemisphere under scenarios of climate change. Global and Planetary Change, 14, 59-72.
15. Romanovsky, V. E., & Osterkamp, T. E. (1997). Thawing of the active layer on the coastal plain of the Alaska Arctic. Permafrost Periglacial Processes, 8, 1-22.
16. Osterkamp, T. E., & Romanovsky, V. E. (1999). Evidence of warming and thawing of discontinuous permafrost in Alaska. PermafrostPeriglacial Processes, 10, 17-37.
17. Clow, G. D., & Urban, F. E. (2002). Large Permafrost Warming in Northern Alaska During the 1990's Determined from GTN-P Borehole Temperature Measurements. American Geophysical

Union, Fall Meeting 2002, Abstract id. B11E-04.

18. Osterkamp, T. E. (2003b). Establishing long-term permafrost observatories for active layer and permafrost investigations in Alaska 1977-2002. Permafrost Periglacial Processes, 14, 331-342.
19. Slater, A. G., & Lawrence, D. M. (2013). Diagnosing Present and Future Permafrost from Climate Models. Journal of Climate, 26, 5608-5623.
20. Pastick, N. J., Jorgenson, M. T., Wylie, B. K., Nield, S. J., Johnson, K. D., & Finley, A. O. (2015). Distribution of near-surface permafrost in Alaska: Estimates of present and future conditions. Remote Sensing of Environment, 168, 301-315.
21. Osterkamp, T. E. (1994). Evidence for warming and thawing of discontinuous permafrost in Alaska. EOS, Transactions of the American Geophysical Union, 75(44): 85.
22. Linell, K. A., & Johnston, G. H. (1973). Engineering Design and Construction in Permafrost Regions: A Review. North American Contribution to the 2nd International Conference on Permafrost (pp. 553-575). National Academy of Sciences.
23. Osterkamp, T. E. (2005). The recent warming of permafrost in Alaska. Global Planet. Change, 49, 187-202.
24. Klene, A. E., Nelson, F. E., Shiklomanov, N. I., & Hinkel, K. M. (2001). The N-Factor in Natural Landscapes: Variability of Air and Soil-Surface Temperatures, Kuparuk River Basin, Alaska, U.S.A. Arctic, Antartic, and Alpine Research, 33(2), 140-148.
25. Klene, A. E., Nelson, F. E., & Shiklomanov, N. I. (2013). The N-Factor as a Tool in Geocryological Mapping: Seasonal Thaw in the Kuparuk River Basin, Alaska. Physical Geography, 22(6), 449-466.
26. Jorgenson, M. T., Yoshikawa, K., Kanveskiy, M., Shur, Y. L., Rornanovsky, V., Marchenko, S., . . .

Brown, I. (2008). Permafrost characteristics of Alaska. Proceedings of the Ninth International Conference on Permafrost, (pp. 121-122). Fairbanks, Alaska.

27. NOAA. (2018). National Climate Data Center. Retrieved October 2018, from National Centers for Environmental Information: National Oceanic and Atmospheric Administration: https://www.ncdc.noaa.gov/cdo-web/datasets.
28. Meehl, G. A., Boer, G. J., Covey, C., Latif, M., & Stouffer, R. J. (2000). The Coupled Model Intercomparison Project (CMIP). Bulletin of the American Meteorological Society, 81, 313-318.
29. IPCC. (2014). Climate Change 2014: Impacts, Adaptation, and Vulnerability. Contribution to the Working Group II. Fifth Assessment Report of the Intergovernmental Panel on Climate Change (AR5).
30. Yarmak, E., & Zottola, J. T. (2017). Thermosyphon Design for a Changing Arctic. Proceedings of the 17th International Conference on Cold Regions Engineering Presented at the 1st Congress on Technical Advancement (pp. 151-160). Congress on Technical Advancement 2017: Cold Regions Engineering.
31. Geoslope. (2019). Temp/W. Calgary, Alberta, Canada. Retrieved from https://www.geoslope.com.
32. Krahn, J. (2004). Thermal modeling with Temp/W: an engineering methodology. Calgary: Geoslope International, Ltd.
33. EBA. (2013). Kuparuk Core Project: Laboratory Results. EBA File: E14103016-01. Technical Report to CPAI, EBA: A Tetra Tech Company.
34. Matthews, C. M., Dessein, T., & Yuen, S. (2015). Comprehensive Thaw Subsidence Assessments for Kuparuk DS-2A Draft Final Report to ConocoPhillips Alaska Inc. C-FER

Technologies, Edmonton, Alberta, Canada.

35. Johansen, O. (1977). Thermal conductivity of soils. Trondheim, Norway: Ph. D. Thesis, CRREL Draft Translation 637.
36. Li, H., Yang, Z., & Wang, J. (2018). Unfrozen water content of permafrost during thawing by the capacitance technique. Cold Regions Science and Technology, 152, 15-22.
37. Lee, Kannon C.. (2019). Assessment of Permafrost Active Layer Thickness and Ground Settlement by Considering Long-Term Climate Impact in Northern Alaska.
38. CALM. (2019). CALM Summary Data Tables. Retrieved from Circumpolar Active Layer Monitoring: https://www2.gwu.edu/~calm/data/north.htm.
39. Cable, W. L., Romanovsky, V. E., & Jorgenson, M. T. (2016). Scaling-up permafrost thermal measurements in western Alaska using an ecotype approach. The Cryosphere, 10, 2517-2532.
40. Nelson, R. A., Luscher, U., & Rooney, J. W. (1983). Thaw strain data and thaw settlement predictions for Alaskan soils. Proceedings of the 4th International Conference on Permafrost, (pp. 912-917). Fairbanks, Alaska.
41. Meehan, R., & Nickles, J. (2002). Oil Development in Northern Alaska: A guide to the effects of gravel placement on wetlands and waterbirds. U.S. Fish and Wildlife Service Alaska Investigations, Environmental Research Laboratory, U.S. EPA.
42. Stephens, J. C., Allen Jr., L. H., & Chen, E. (1984). Organic Soil Subsidence. In T. L. Holzer, Man-Induced Land Subsidence (Vol. 6). The Geological Society of America.
43. Esch, D. C., & Osterkamp, T. E. (1990). Cold Regions Engineering: Climatic Warming Concerns for Alaska. Cold Regions Engineering, 4(1), 6-14.
44. McBeath, J. (2003). Institutional responses to climate change: the case of the Alaska

transportation system. Mitigation and Adaptation Strategies for Global Change, 8(3-28), 3-28.

## Declarations

### Availability of data and materials

The datasets used and/or analysed during the current study are available from the corresponding author on reasonable request.

### Competing interests

The authors declare that they have no competing interests.

### Funding

This study is financially support by a grant from the ConocoPhillips Arctic Science and Engineering Endowment.

### Authors' contributions

ZY drafted this manuscript and guided the analysis of climate data, thermal modeling and settlement prediction. KL analyzed and interpreted the climate data, conducted the thermal modeling and ground settlement prediction. HL retrieved and assisted in analyzing the climate prediction data.

### Acknowledgments

We are thankful to Conoco Phillips, Alaska, for their generous donation of permafrost cores.

# Figures


**Figure 1**

Location of study site on Alaska's North Slope. Note: The designations employed and the presentation of the material on this map do not imply the expression of any opinion whatsoever on the part of Research Square concerning the legal status of any country, territory, city or area or of its authorities, or concerning the delimitation of its frontiers or boundaries. This map has been provided by the authors.

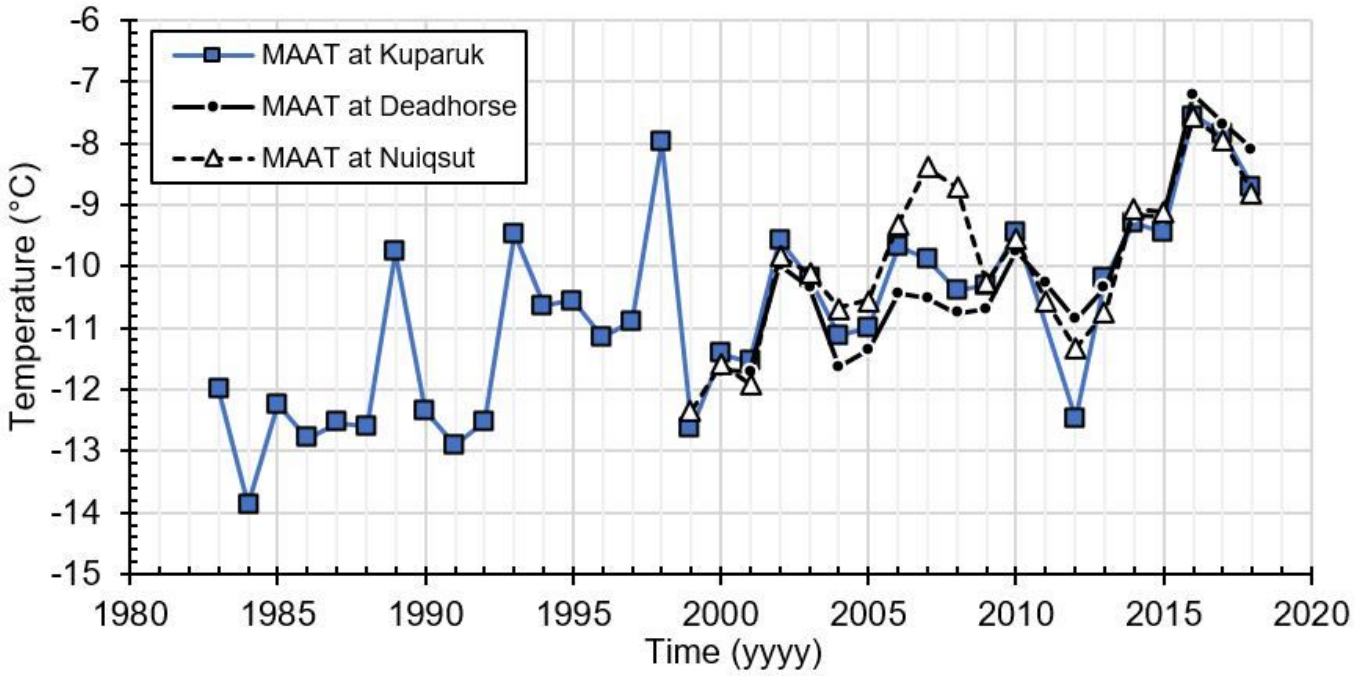

## Figure 2

Mean annual air temperature comparison between locations indicating similar increasing temperature trends.

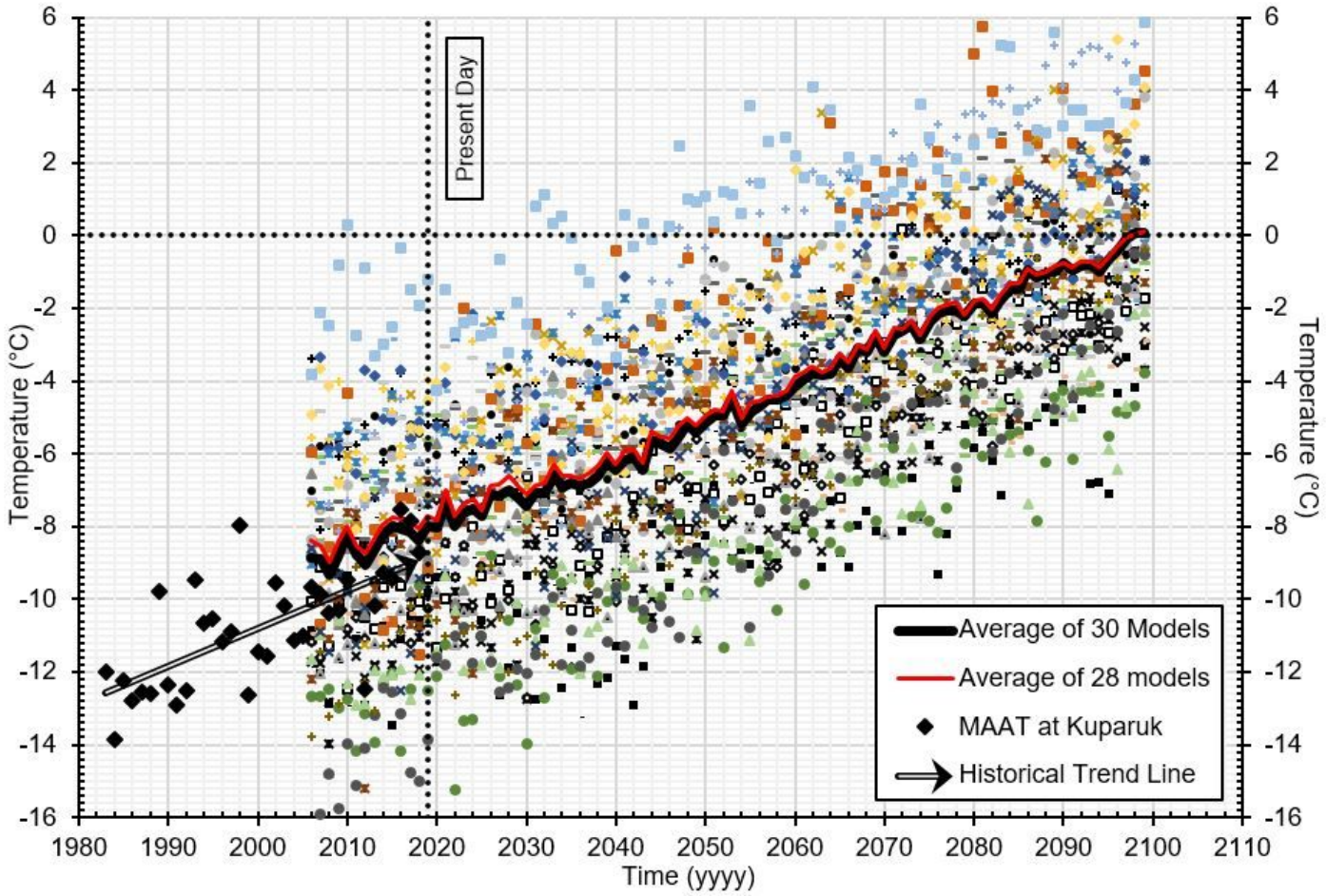


## Figure 3

Historical and predicted mean annual air temperature at the study site. The various colored dots represent 1 of the 30 climate models in this study. The average of all models was used in the thermal modeling.

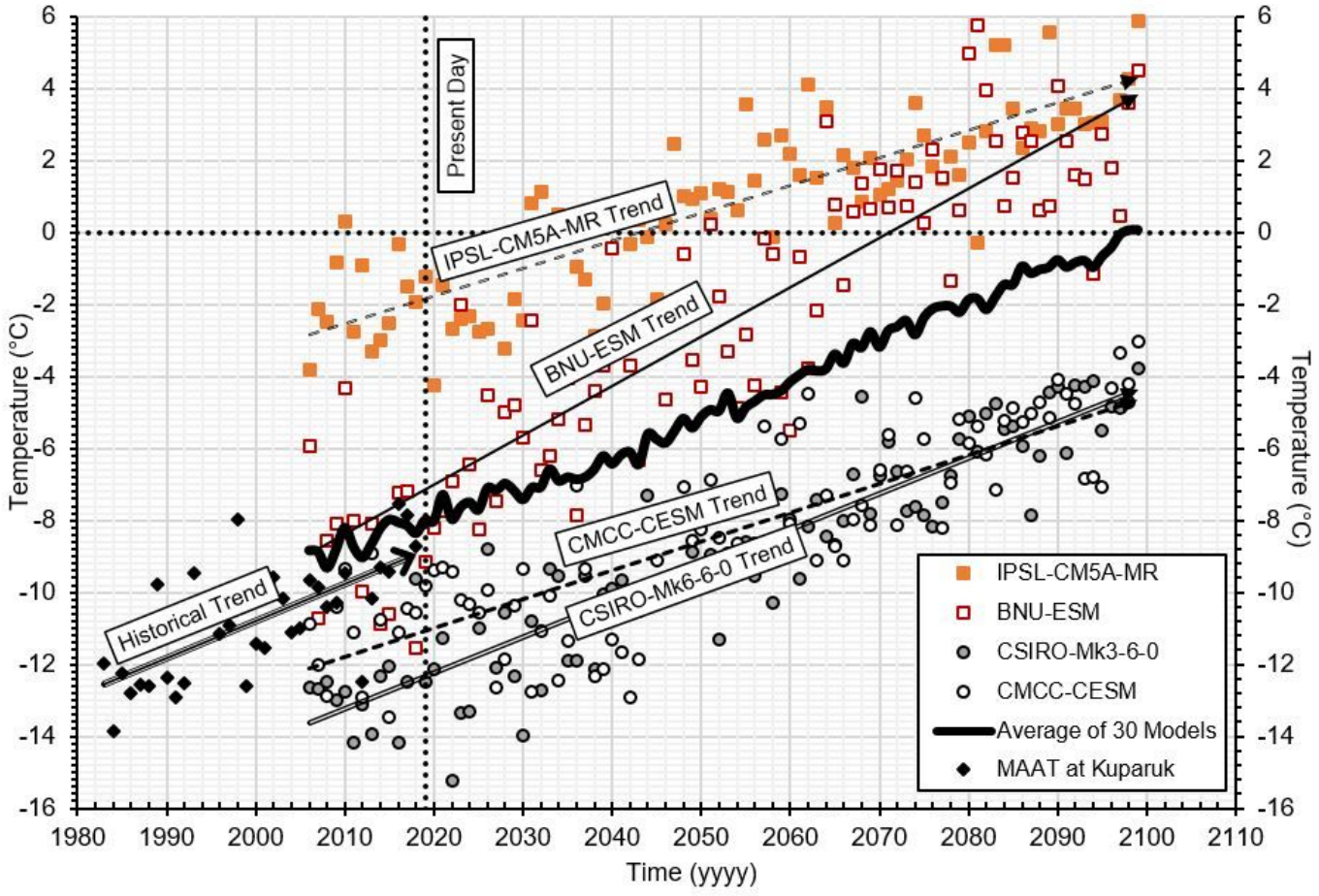


**Figure 4**

Predicted mean annual air temperature of the upper and lower bounds of the 30 climate models showing trends of four models with historical and predicted averages.

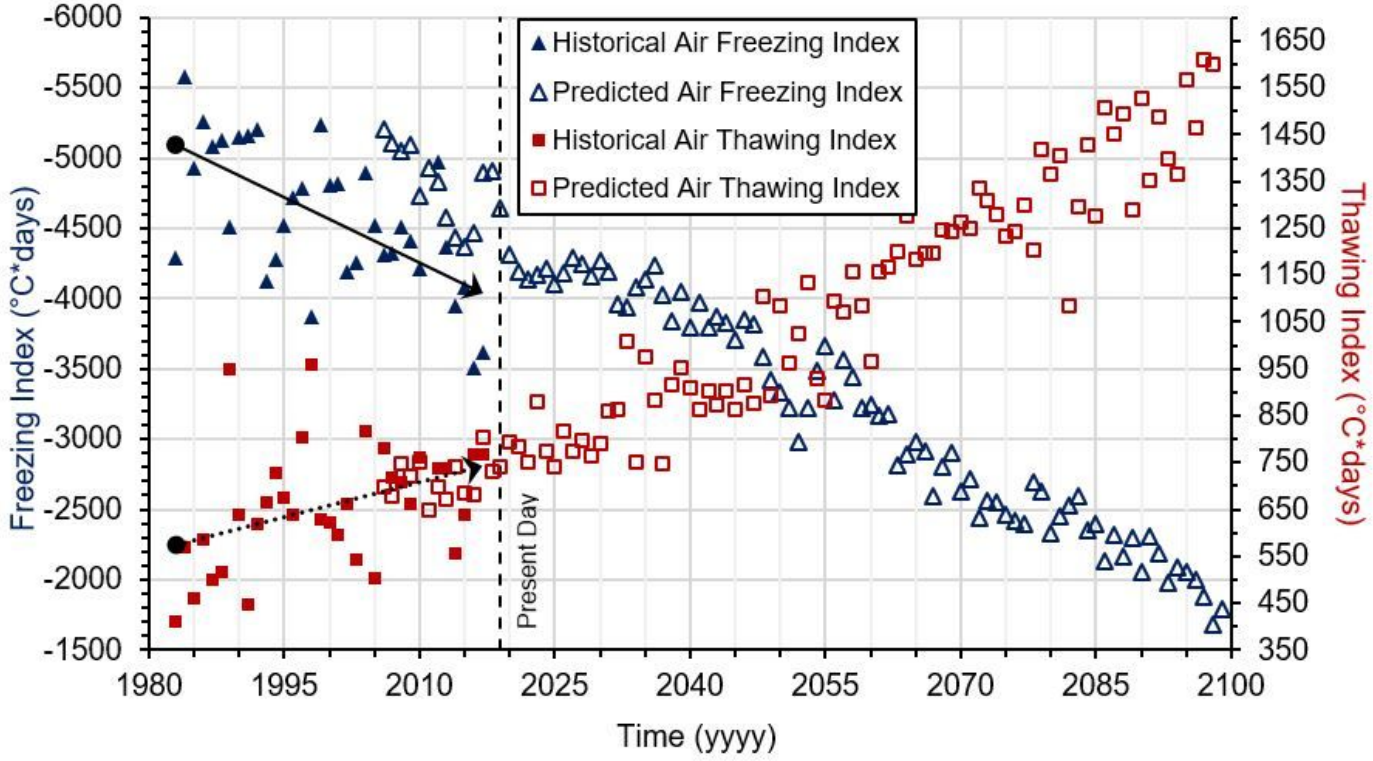


**Figure 5**

Historical and predicted air freezing and thawing indices.

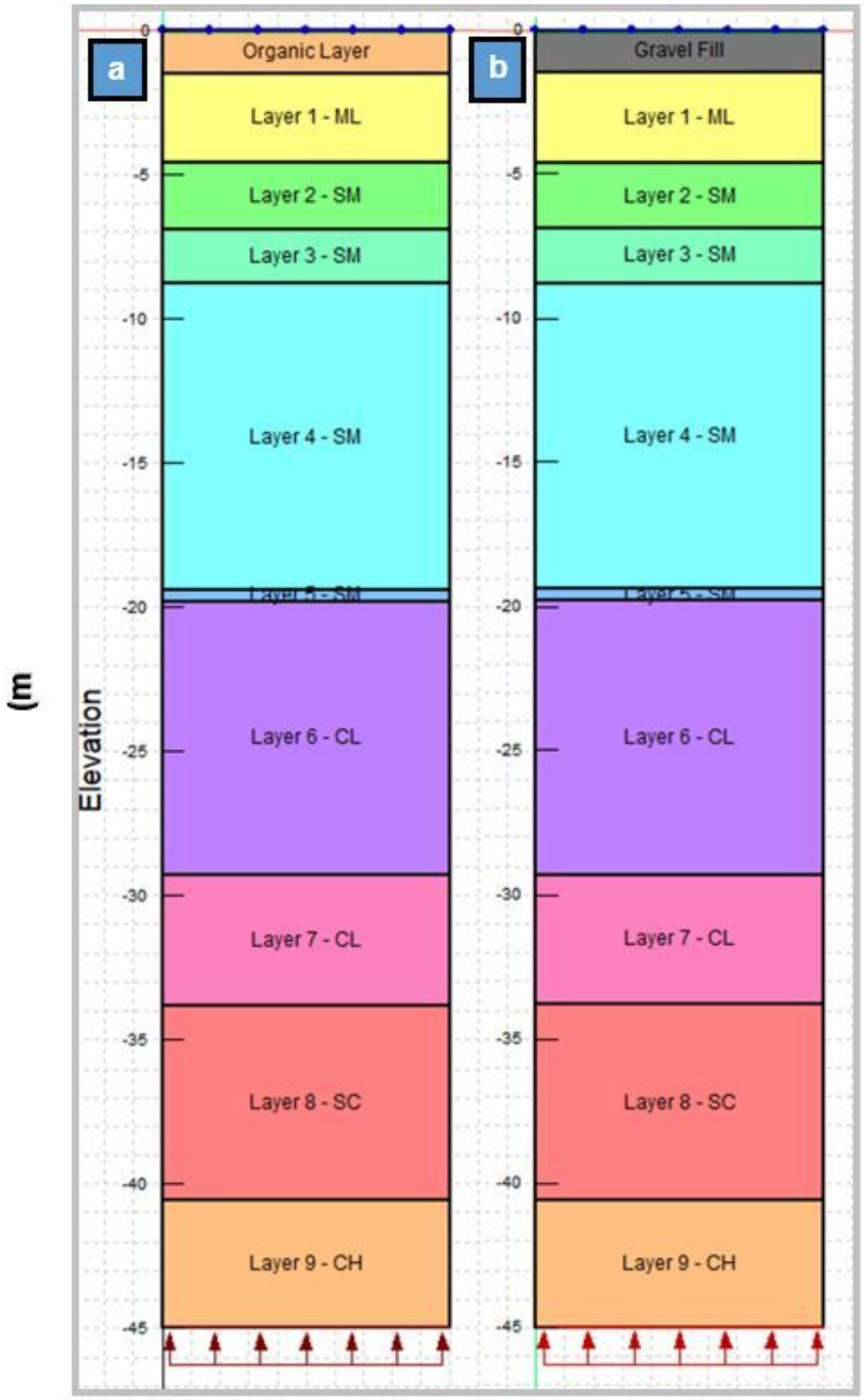


**Figure 6**

Comparison of two TEMP/W models: a) with an organic layer at the surface, b) with a gravel layer at the surface.

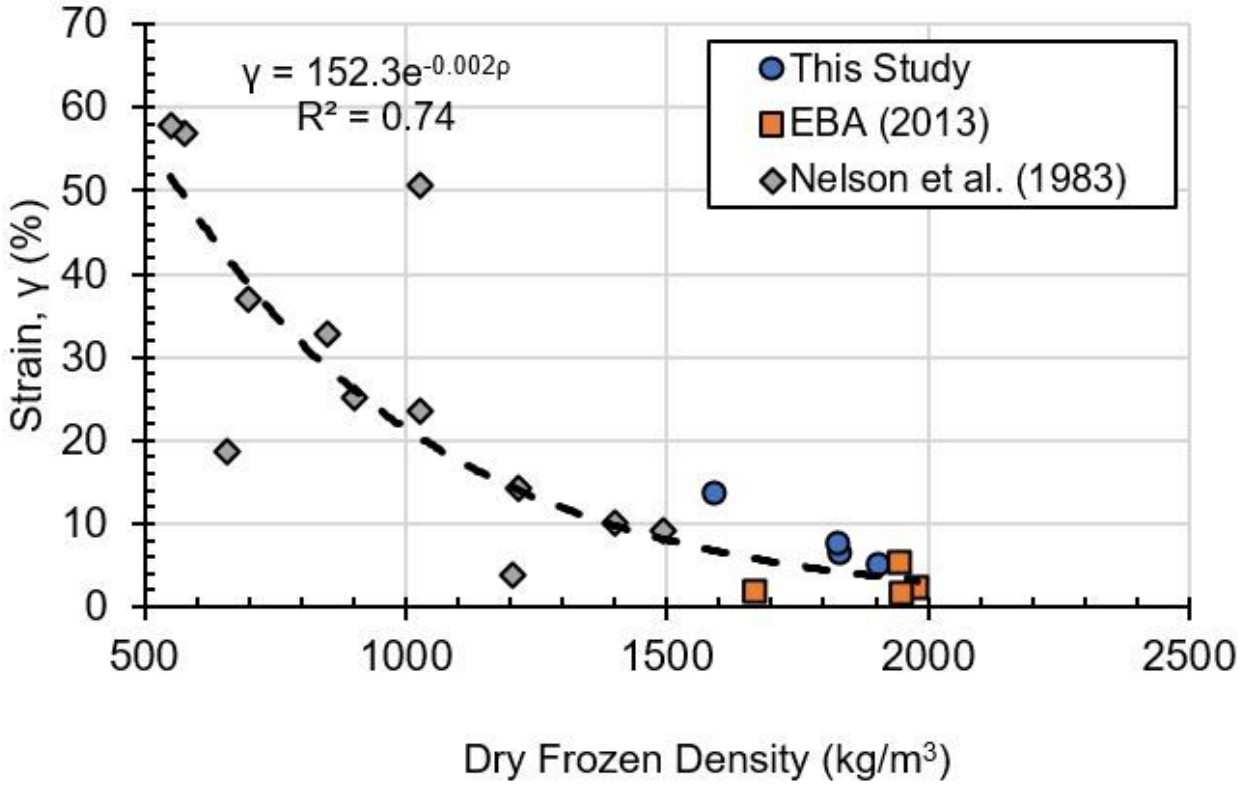


**Figure 7**

Percent strain as related to dry frozen density for silt and clay.

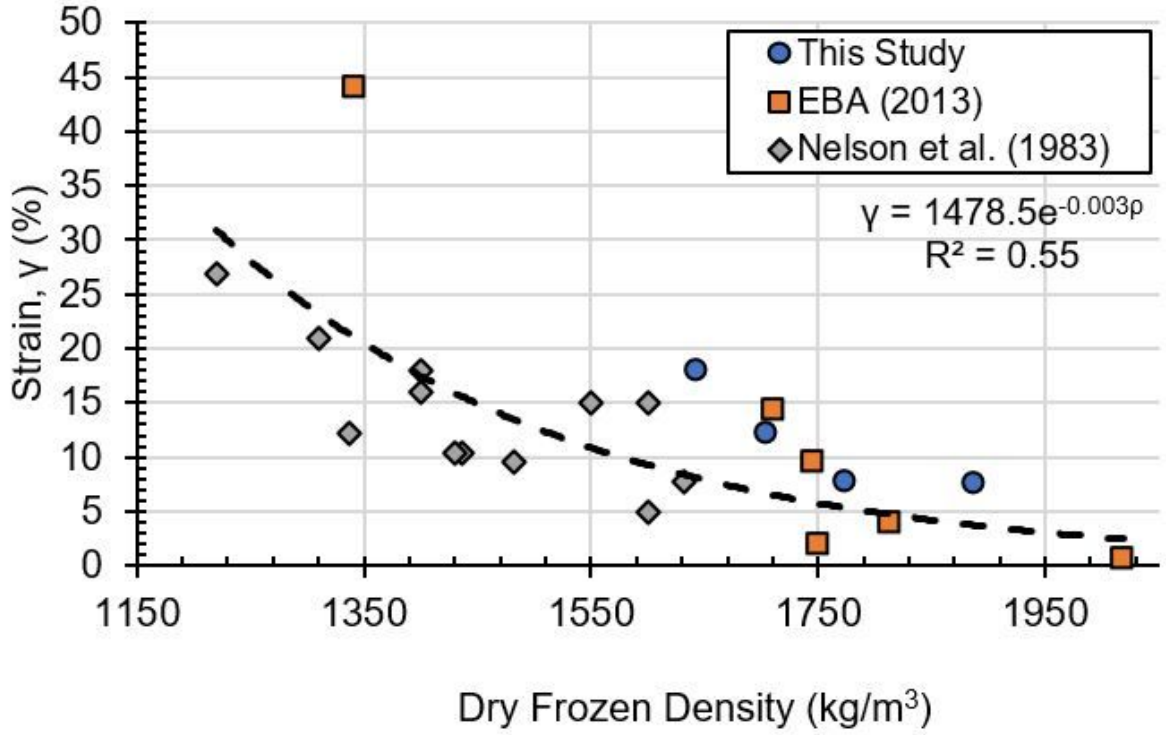

**Figure 8**

Percent strain as related to dry frozen density for sand and silty sand.

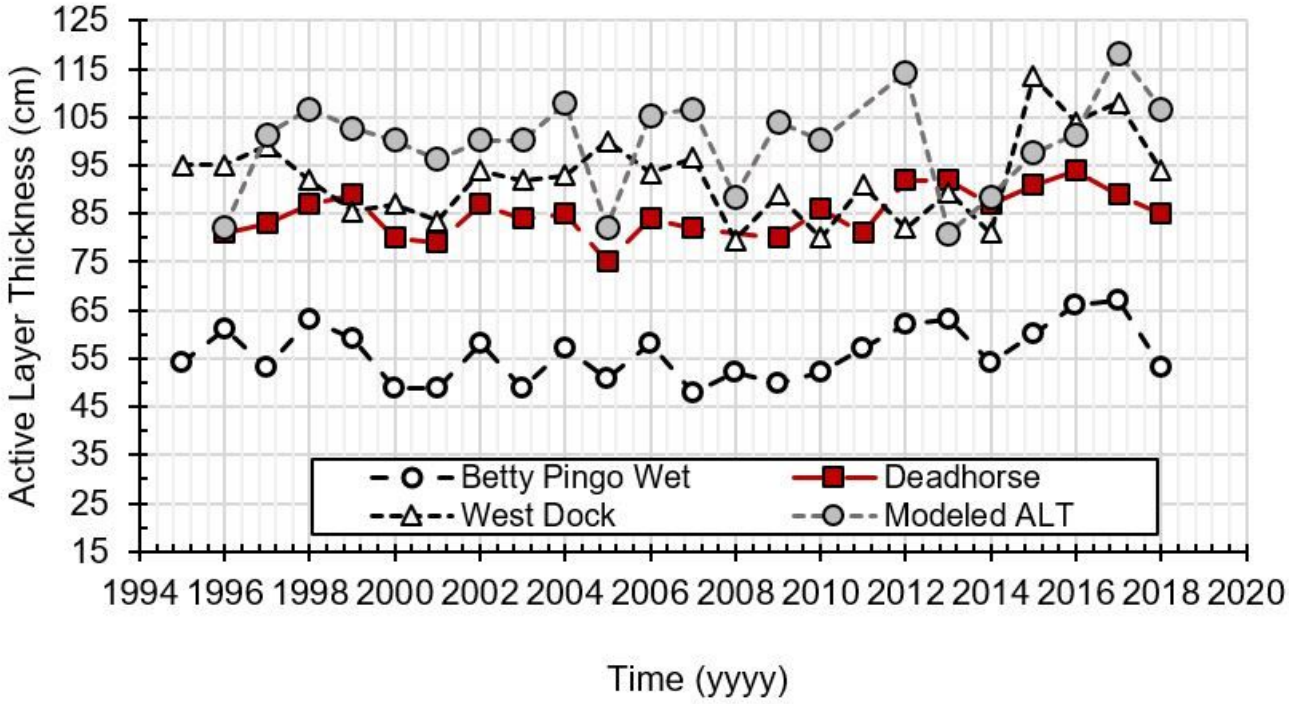


**Figure 9**

Comparison of measured and modeled ALT.

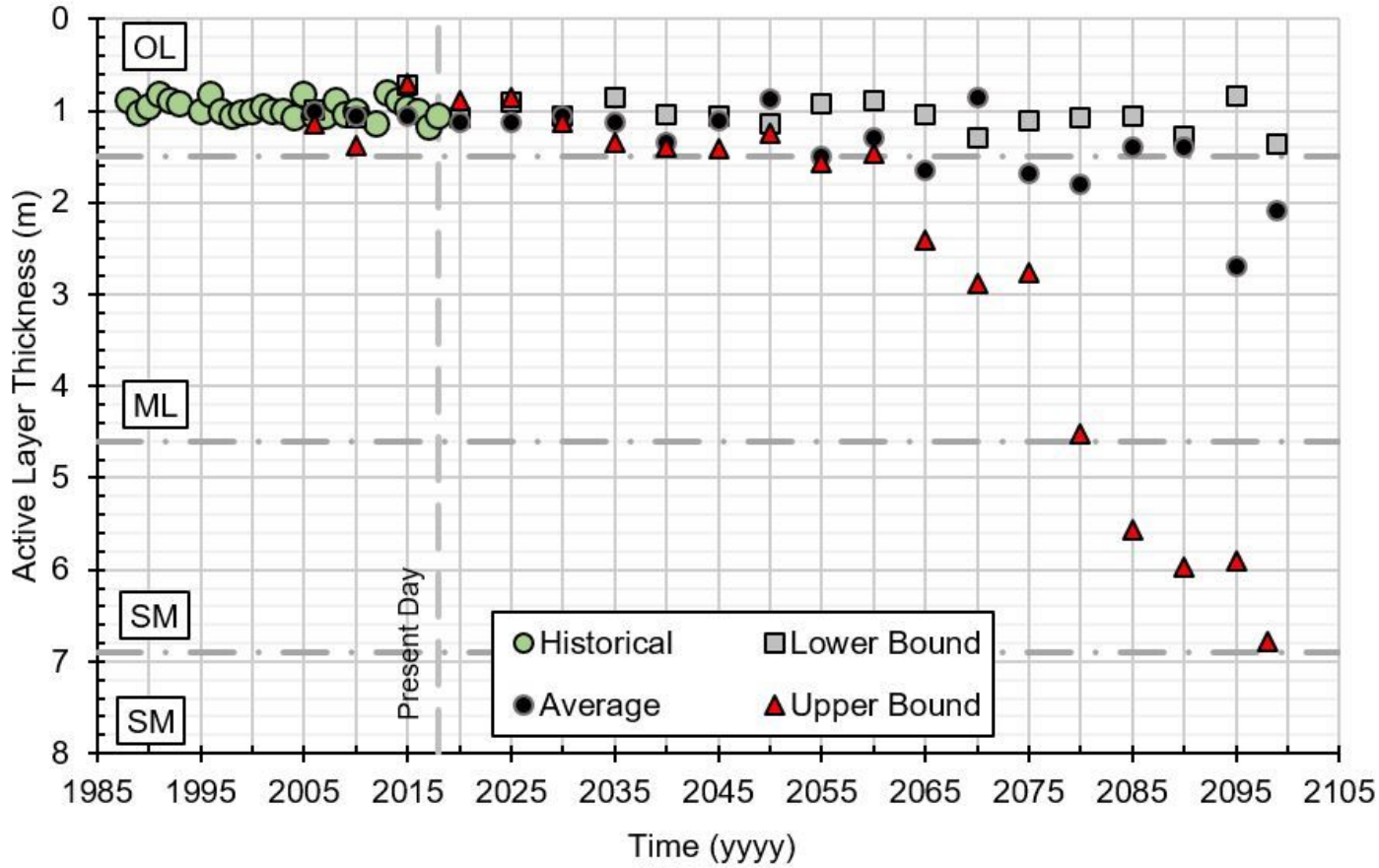


**Figure 10**

Modeled ALT from 1988 to 2100 for undisturbed tundra. Scenarios 1, 2, and 3 are represented by Average, Upper Bound, and Lower Bound in the figure, respectively.

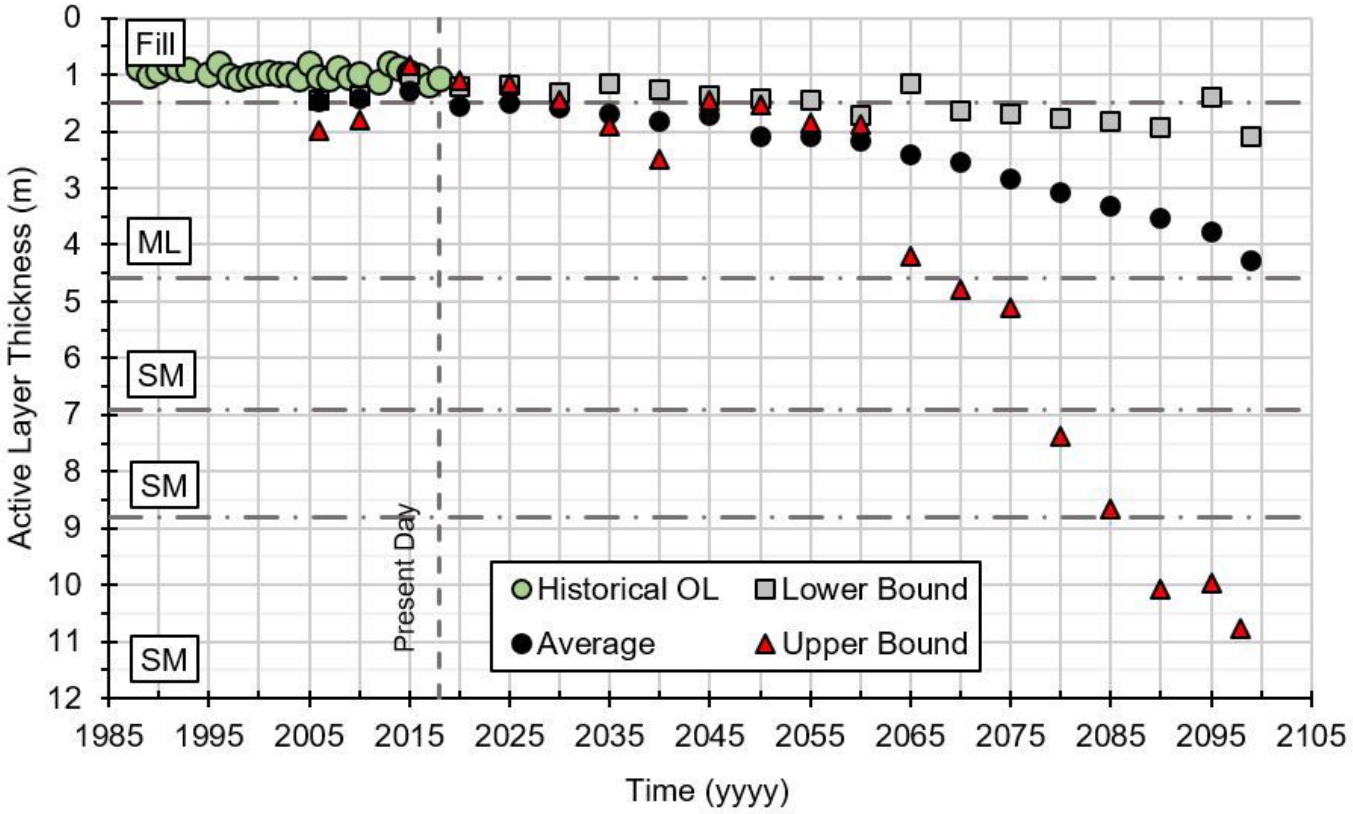


**Figure 11**

Modeled ALT when a gravel pad is emplaced at the site, with development occurring in 2006. The modeled historical organic layer ALT is provided for reference. Scenarios 1, 2, and 3 are represented by Average, Upper Bound, and Lower Bound in the figure, respectively.

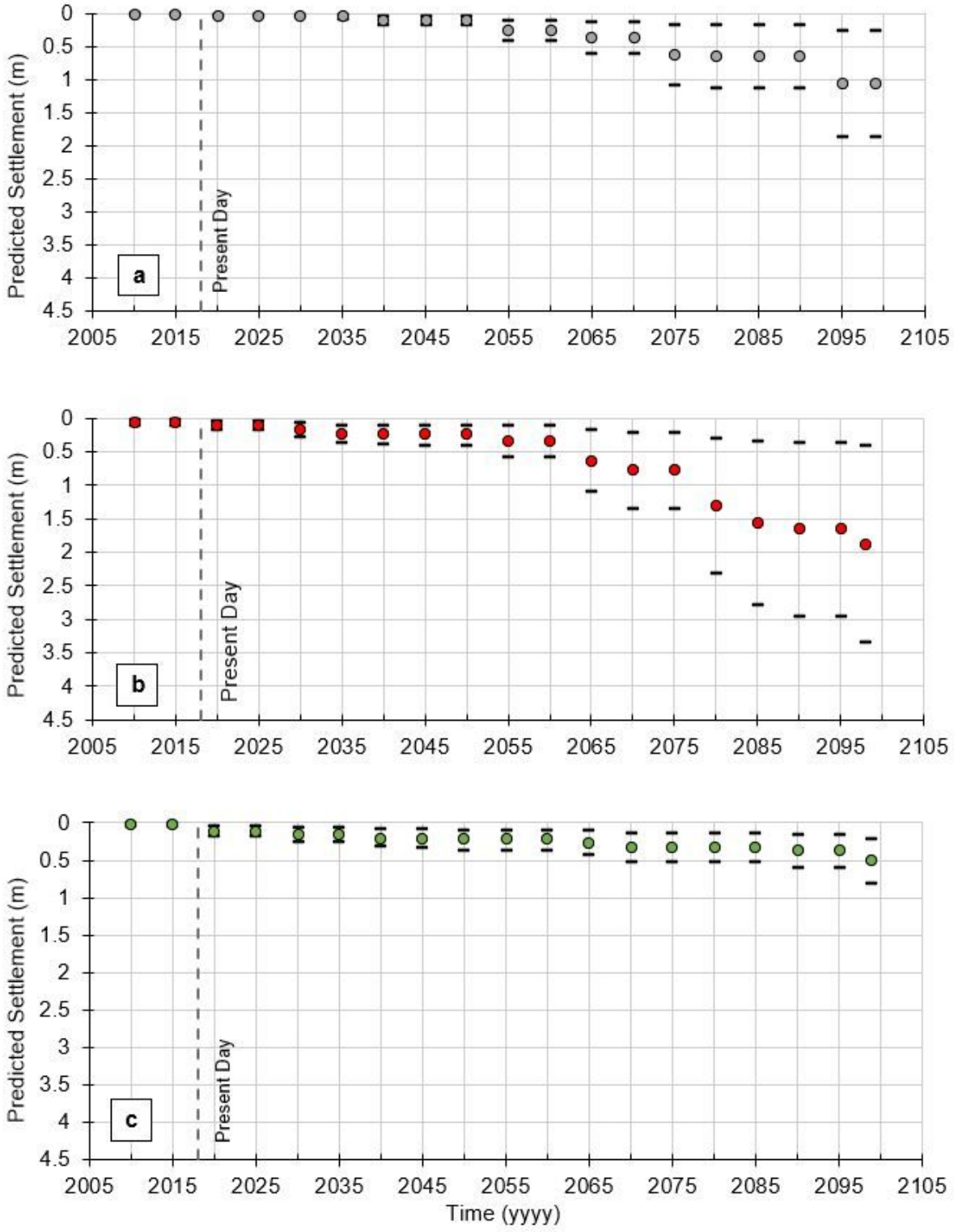


**Figure 12**

Predicted settlement at the study site due to active layer thickening under undisturbed ground surface conditions: (a) 28 Climate Model Average; (b) BNU-ESM upper bound climate model; (c) CMCC-CESM lower bound climate model. The dashed vertical line at 2018 indicates the present day for reference.

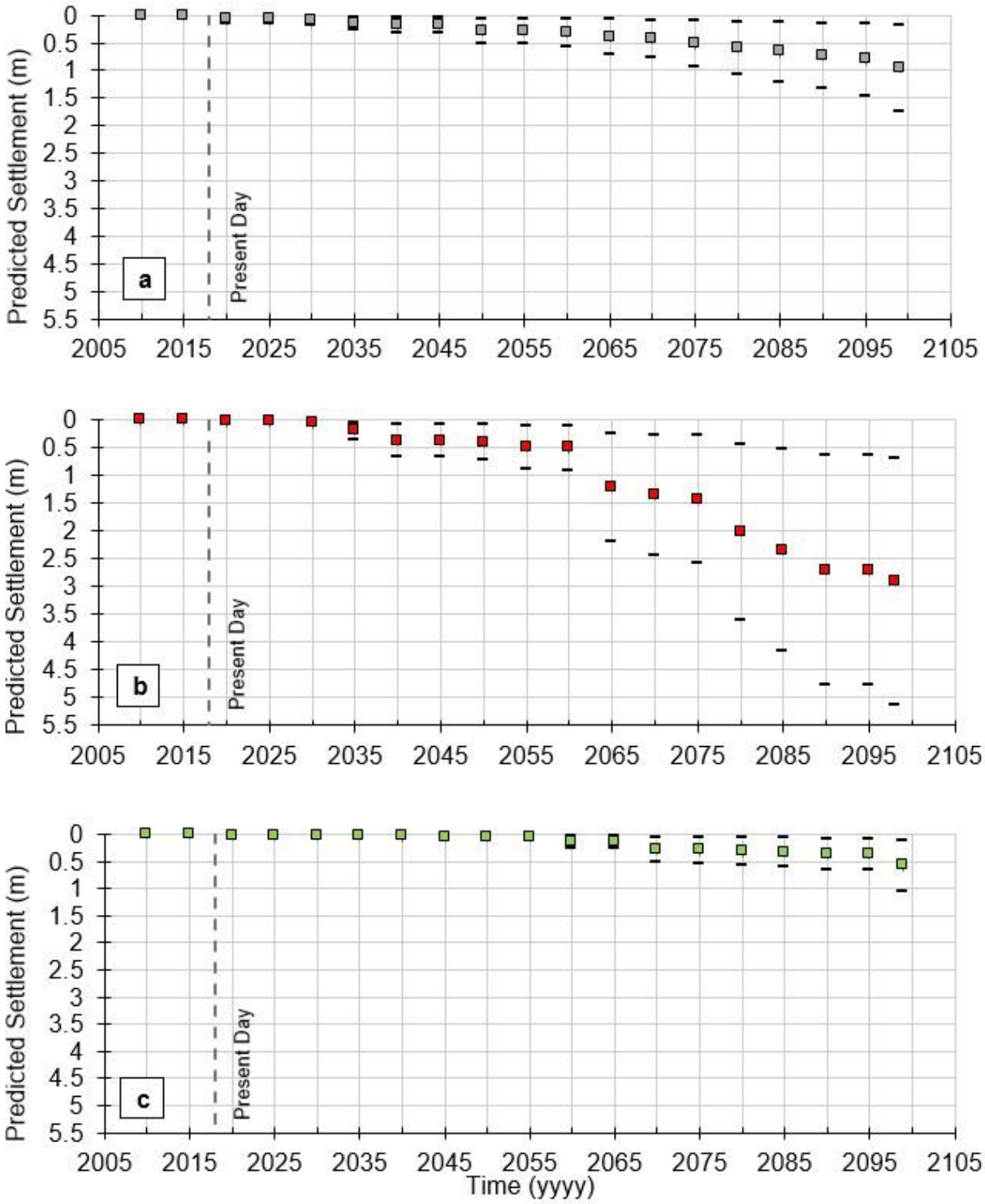


**Figure 13**

Predicted settlement at the study site due to active layer thickening under disturbed ground surface conditions where the organic layer was replaced with gravel fill: (a) 28 climate model average; (b) BNU-ESM upper bound climate model; (c) CMCC-CESM lower bound climate model.